11

Laser Beam Diagnostics in a Spatial Domain

Tae Moon Jeong and Jongmin Lee
Advanced Photonics Research Institute,
Gwangju Institute of Science and Technology
Korea

1. Introduction

The intensity distribution of laser beams in the focal plane of a focusing optic is important because it determines the laser-matter interaction process. The intensity distribution in the focal plane is determined by the incoming laser beam intensity and its wavefront profile. In addition to the intensity distribution in the focal plane, the intensity distribution near the focal plane is also important. For a simple laser beam having a Gaussian or flat-top intensity profile, the intensity distribution near the focal plane can be analytically described. In many cases, however, the laser beam profile cannot be simply described as either Gaussian or flat-top. To date, many researchers have attempted to characterize laser beam propagation using a simple metric for laser beams having an arbitrary beam profile. With this trial, researchers have devised a beam quality (or propagation) factor capable of describing the propagation property of a laser beam, especially near the focal plane. Although the beam quality factor is not a magic number for characterizing the beam propagation, it can be widely applied to characterizing the propagation of a laser beam and is also able to quickly estimate how small the size of the focal spot can reach. In this chapter, we start by describing the spatial profile of laser beams. In Section 2, the derivation of the spatial profile of laser beams will be reviewed for Hermite-Gaussian, Laguerre-Gaussian, super-Gaussian, and Bessel-Gaussian beam profiles. Then, in Section 3, the intensity distribution near the focal plane will be discussed with and without a wavefront aberration, which is another important parameter for characterizing laser beams. Although the Shack-Hartmann wavefront sensor is widely used for measuring the wavefront aberration of a laser beam, several other techniques to measure a wavefront aberration will be introduced. Knowing the intensity distributions near the focal plane enables us to calculate the beam quality (propagation) factor. In Section 4, we will review how to determine the beam quality factor. In this case, the definition of the beam quality factor is strongly related to the definition of the radius of the intensity distribution. For a Gaussian beam profile, defining the radius is trivial; however, for an arbitrary beam profile, defining the beam radius is not intuitively simple. Here, several methods for defining the beam radius are introduced and discussed. The experimental procedure for measuring the beam radius will be introduced and finally determining the beam quality factor will be discussed in terms of experimental and theoretical methods.

2. Spatial beam profile of the laser beam

In this section, we will derive the governing equation for the electric field of a laser beam. The derived electric field has a special distribution, referred to as beam mode, determined

by the boundary conditions. Two typical laser beam modes are Hermite-Gaussian and Laguerre-Gaussian modes. In this chapter, we also introduce two other beam modes: top-hat (or flat-top) and Bessel-Gaussian beam modes. These two beam modes become important when considering high-power laser systems and diffraction-free laser beams. These laser beam modes can be derived from Maxwell's equations.

2.1 Derivation of the beam profile

When the laser beam propagates in a source-free (means charge- and current-free) medium, Maxwell's equations in Gaussian units are:

$$\nabla \times \vec{E} + \frac{1}{c}\frac{\partial \vec{B}}{\partial t} = 0 , \tag{2.1}$$

$$\nabla \times \vec{H} - \frac{1}{c}\frac{\partial \vec{D}}{\partial t} = 0 , \tag{2.2}$$

$$\nabla \cdot \vec{D} = 0 , \tag{2.3}$$

$$\text{and } \nabla \cdot \vec{B} = 0 \tag{2.4}$$

where $\vec{E}$ and $\vec{H}$ are electric and magnetic fields. In addition, $\vec{D}$ and $\vec{B}$ are electric and magnetic flux densities defined as

$$\vec{D} = \vec{E} + 4\pi\vec{P} \text{ and } \vec{B} = \vec{H} + 4\pi\vec{M} . \tag{2.5}$$

Polarization and magnetization densities ($\vec{P}$ and $\vec{M}$) are then introduced to define the electric and magnetic flux densities as follows:

$$\vec{P} = \chi\vec{E} \text{ and } \vec{M} = \eta\vec{H} . \tag{2.6}$$

As such, the electric and magnetic flux densities can be simply expressed as

$$\vec{D} = \varepsilon\vec{E} \text{, and } \vec{B} = \mu\vec{H} . \tag{2.7}$$

where ε and μ are the electric permittivity and magnetic permeability, respectively. Note that if there is an interface between two media, $\vec{E}$, $\vec{H}$, $\vec{D}$, and $\vec{B}$ should be continuous at the interface. This continuity is known as the continuity condition at the media interface. To be continuous, $\vec{E}$, $\vec{H}$, $\vec{D}$, and $\vec{B}$ should follow equation (2.8).

$$\hat{n} \times \left(\vec{E}_2 - \vec{E}_1\right) = 0 , \ \hat{n} \times \left(\vec{H}_2 - \vec{H}_1\right) = 0 , \ \hat{n} \cdot \left(\vec{D}_2 - \vec{D}_1\right) = 0 \text{, and } \hat{n} \cdot \left(\vec{B}_2 - \vec{B}_1\right) = 0 \tag{2.8}$$

Next, using equation (2.5), and taking $\nabla\times$ in equations (2.1) and (2.2), equations for the electric and magnetic fields become

$$\nabla \times \nabla \times \vec{E} + \frac{1}{c^2}\frac{\partial^2 \vec{E}}{\partial t^2} = -\frac{4\pi}{c}\frac{\partial}{\partial t}\left[\frac{1}{c}\frac{\partial \vec{P}}{\partial t} + \nabla \times \vec{M}\right], \tag{2.9}$$

$$\text{and } \nabla\times\nabla\times\vec{H}+\frac{1}{c^2}\frac{\partial^2\vec{H}}{\partial t^2}=\frac{4\pi}{c}\left[\nabla\times\frac{\partial\vec{P}}{\partial t}-\frac{1}{c}\frac{\partial^2\vec{M}}{\partial t^2}\right]. \tag{2.10}$$

Because the electric and magnetic fields behave like harmonic oscillators having a frequency ω in the temporal domain, $\frac{\partial}{\partial t}$ can be replaced with $-i\omega$. Then, using the relation $k=\frac{\omega}{c}$ (c is the speed of light), equations (2.9) and (2.10) become

$$\nabla\times\nabla\times\vec{E}(\vec{r})-k^2\vec{E}(\vec{r})=4\pi\left[k^2\vec{P}(\vec{r})+ik\nabla\times\vec{M}(\vec{r})\right], \tag{2.11}$$

$$\text{and } \nabla\times\nabla\times\vec{H}(\vec{r})-k^2\vec{H}(\vec{r})=4\pi\left[-ik\nabla\times\vec{P}(\vec{r})+k^2\vec{M}(\vec{r})\right]. \tag{2.12}$$

If we assume that the electromagnetic field propagates in free space (vacuum), then polarization and magnetization densities ($\vec{P}$ and $\vec{M}$) are zero. Thus, the right sides of equations (2.11) and (2.12) become zero, and finally,

$$\nabla\times\nabla\times\vec{E}(\vec{r})-k^2\vec{E}(\vec{r})=0, \tag{2.13}$$

$$\text{and } \nabla\times\nabla\times\vec{H}(\vec{r})-k^2\vec{H}(\vec{r})=0. \tag{2.14}$$

By using a BAC-CAB rule in the vector identity, equation (2.13) for the electric field becomes

$$\nabla\nabla\cdot\vec{E}(\vec{r})-\nabla\cdot\nabla\vec{E}-k^2\vec{E}(\vec{r})=0. \tag{2.15}$$

We will only consider the electric field because all characteristics for the magnetic field are the same as those for the electric field, except for the magnitude of the field. Because the source-free region is considered, the divergence of the electric field is zero ($\nabla\cdot\vec{E}(\vec{r})=0$). Finally, the expression for the electric field is given by

$$\nabla\cdot\nabla\vec{E}+k^2\vec{E}(\vec{r})=0. \tag{2.16}$$

This is the general wave equation for the electric field that governs the propagation of the electric field in free space. In many cases, the propagating electric field (in the z-direction in rectangular coordinates) is linearly polarized in one direction (such as the x- or y-direction in rectangular coordinates). As for a linearly x-polarized propagating electric field, the electric field propagating in the z-direction can be expressed in rectangular coordinates as

$$\vec{E}(\vec{r})=\hat{i}E_0(x,y,z)\exp(ikz). \tag{2.17}$$

By substituting equation (2.17) into equation (2.18), the equation becomes

$$\left(\frac{\partial^2}{\partial x^2}+\frac{\partial^2}{\partial y^2}+\frac{\partial^2}{\partial z^2}\right)\hat{i}E_0(x,y,z)\exp(ikz)+\hat{i}k^2E_0(x,y,z)\exp(ikz)=0. \tag{2.18}$$

Equation (2.18) is referred to as a homogeneous Helmholtz equation, which describes the wave propagation in a source-free space. By differentiating the wave in the z-coordinate, we obtain

$$\frac{\partial}{\partial z}E_0(x,y,z)\exp(ikz) = ikE_0(x,y,z)\exp(ikz) + \frac{\partial E_0(x,y,z)}{\partial z}\exp(ikz), \tag{2.19}$$

and

$$\frac{\partial^2}{\partial z^2}E_0(x,y,z)\exp(ikz) = -k^2E_0(x,y,z)\exp(ikz) + 2ik\frac{\partial E_0(x,y,z)}{\partial z}\exp(ikz) + \frac{\partial^2 E_0(x,y,z)}{\partial z^2}\exp(ikz). \tag{2.20}$$

In many cases, the electric field slowly varies in the propagation direction (z-direction). The slow variation of the electric field in z-direction can make possible the following approximation (slowly varying approximation):

$$\left|\frac{\partial^2 E_0(x,y,z)}{\partial z^2}\right| \ll 2\left|k\frac{\partial E_0(x,y,z)}{\partial z}\right|. \tag{2.21}$$

By inserting equation (2.20) into equation (2.18) and using the assumption of equation (2.21), equation (2.18) becomes

$$\frac{\partial^2 E_0(x,y,z)}{\partial x^2} + \frac{\partial^2 E_0(x,y,z)}{\partial y^2} + 2ik\frac{\partial E_0(x,y,z)}{\partial z} = 0. \tag{2.22}$$

Equation (2.22) describes how the linearly polarized electric field propagates in the z-direction in the Cartesian coordinate.

2.2 Hermite-Gaussian beam mode in rectangular coordinate

In the previous subsection, we derived the equation for describing the propagation of a linearly polarized electric field. Now, the question is how to solve the wave equation and what are the possible electric field distributions. In this subsection, the electric field distribution will be derived as a solution of the wave equation (2.22) with a rectangular boundary condition. Consequently, the solution of the wave equation in the rectangular coordinate has the form of a Hermite-Gaussian function. Thus, the laser beam mode is referred to as Hermite-Gaussian mode in the rectangular coordinate; the lowest Hermite-Gaussian mode is Gaussian, which commonly appears in many small laser systems.

Now, let us derive the Hermite-Gaussian beam mode in the rectangular coordinate. The solution of equation (2.22) in rectangular coordinates was found by Fox and Li in 1961. In that literature, they assume that a trial solution to the paraxial equation has the form

$$E_0(x,y,z) = A(z)\times\exp\left[-ik\frac{x^2+y^2}{2q(z)}\right] \tag{2.23}$$

where A(z) is the electric field distribution in z-coordinate and $q(z)$ is the general expression for the radius of the wavefront of the electric field to be determined. For the time being, let us assume that the electric field distribution in x- and y-coordinates is constant. Then, if $q(z)$ is complex-valued, $q(z)$ can be expressed with real and imaginary parts as follows:

$$\frac{1}{q(z)} = \frac{1}{q_r(z)} - i\frac{1}{q_i(z)}. \tag{2.24}$$

By inserting equation (2.24) into equation (2.23), the resulting equation will be

$$E_0(x,y,z) = A(z) \times \exp\left[-ik\frac{x^2+y^2}{2q_r(z)}\right] \times \exp\left[-k\frac{x^2+y^2}{2q_i(z)}\right]. \tag{2.25}$$

The real part of equation (2.25) determines the magnitude distribution of the electric field and the imaginary part gives the spatial phase or wavefront profile. In a specific case such as the Gaussian beam profile, $q_i(z)$ determines the radius of the Gaussian beam, defined as

$$q_i(z) = \frac{\pi w^2(z)}{\lambda} \tag{2.26}$$

where $w(z)$ is the radius of the Gaussian beam profile. By calculating $\frac{\partial}{\partial x}$, $\frac{\partial}{\partial y}$, $\frac{\partial^2}{\partial x^2}$, $\frac{\partial^2}{\partial y^2}$, and $\frac{\partial}{\partial z}$ using equation (2.23), we can obtain

$$\frac{\partial E_0}{\partial x} = -ik\frac{x}{q(z)} \times A(z) \times \exp\left[-ik\frac{x^2+y^2}{2q(z)}\right], \tag{2.27}$$

$$\frac{\partial E_0}{\partial y} = -ik\frac{y}{q(z)} \times A(z) \times \exp\left[-ik\frac{x^2+y^2}{2q(z)}\right], \tag{2.28}$$

$$\frac{\partial^2 E_0}{\partial x^2} = -ik\frac{A(z)}{q(z)} \times \exp\left[-ik\frac{x^2+y^2}{2q(z)}\right] - k^2\frac{x^2}{q^2(z)}A(z) \times \exp\left[-ik\frac{x^2+y^2}{2q(z)}\right], \tag{2.29}$$

$$\frac{\partial^2 E_0}{\partial y^2} = -ik\frac{A(z)}{q(z)} \times \exp\left[-ik\frac{x^2+y^2}{2q(z)}\right] - k^2\frac{y^2}{q^2(z)}A(z) \times \exp\left[-ik\frac{x^2+y^2}{2q(z)}\right], \tag{2.30}$$

and

$$\frac{\partial E_0}{\partial z} = \frac{dA(z)}{dz} \times \exp\left[-ik\frac{x^2+y^2}{2q(z)}\right] + ikA(z)\frac{x^2+y^2}{2q^2(z)}\frac{dq(z)}{dz} \times \exp\left[-ik\frac{x^2+y^2}{2q(z)}\right]. \tag{2.31}$$

And, by inserting equations (2.27)–(2.31) into equation (2.22), equation (2.22) becomes

$$\left[k^2\left(\frac{dq(z)}{dz}-1\right)\frac{x^2+y^2}{q^2(z)}-\frac{2ik}{q(z)}\left(\frac{q(z)}{A(z)}\frac{dA(z)}{dz}+1\right)\right]A(z)=0\,. \tag{2.32}$$

All relations in the parentheses on the left side of equation (2.32) should be zero in order to satisfy the above equation for any condition, i.e.

$$\frac{dq(z)}{dz}=1 \text{ and } \frac{q(z)}{A(z)}\frac{dA(z)}{dz}=-1 \text{ or } \frac{dA(z)}{A(z)}=-\frac{dz}{q(z)}=-\frac{dq(z)}{q(z)}\frac{dz}{dq(z)}=-\frac{dq(z)}{q(z)}\,. \tag{2.33}$$

By integrating equation (2.33), the following relationship is obtained:

$$q(z)=q(z_0)+z-z_0 \text{ and } \frac{A(z)}{A(z_0)}=\frac{q(z_0)}{q(z)}\,. \tag{2.34}$$

Now, let us consider the case that the electric field has a distribution in the x- and y-directions. In this case, it is convenient to separate variables and the electric field can be rewritten as

$$E_0(x,y,z)=E_{mn}(x,y,z)=A(z)E_m(x)E_n(y)=A\left[q(z)\right]E_m(x)E_n(y)\,. \tag{2.35}$$

Here, if we only consider the electric field in x-z plane, then

$$E(x,z)=A\left[q(z)\right]\times E_m(x)\times\exp\left[-ik\frac{x^2}{2q(z)}\right]. \tag{2.36}$$

And by differentiating the electric field, we obtain

$$\begin{aligned}\frac{\partial^2}{\partial x^2}E(x)=&A\left[q(z)\right]\times\frac{\partial^2}{\partial x^2}E_m(x)\times\exp\left[-ik\frac{x^2}{2q(z)}\right]\\&+2A\left[q(z)\right]\times\frac{\partial}{\partial x}E_m(x)\times\left[-ik\frac{x}{q(z)}\right]\times\exp\left[-ik\frac{x^2}{2q(z)}\right]\\&+A\left[q(z)\right]\times E_m(x)\times\left[-ik\frac{1}{q(z)}\right]\times\exp\left[-ik\frac{x^2}{2q(z)}\right]\\&+A\left[q(z)\right]\times E_m(x)\times\left[-k^2\frac{x^2}{q^2(z)}\right]\times\exp\left[-ik\frac{x^2}{2q(z)}\right]\end{aligned}, \tag{2.37}$$

and

$$\frac{\partial}{\partial z}E(x,z)=\frac{d}{dq}A\left[q(z)\right]\times E_m(x)\times\exp\left[-ik\frac{x^2}{2q(z)}\right]+A\left[q(z)\right]\times E_m(x)\times\left[ik\frac{x^2}{2q^2(z)}\right]\times\exp\left[-ik\frac{x^2}{2q(z)}\right]. \tag{2.38}$$

By inserting equations (2.37) and (2.38) into equation (2.22), we obtain

$$\frac{\partial^2}{\partial x^2}E_m(x)-2ik\frac{x}{q(z)}\frac{\partial}{\partial x}E_m(x)+ik\left[\frac{2}{A\left[q(z)\right]}\frac{d}{dq}A\left[q(z)\right]-\frac{1}{q(z)}\right]E_m(x)=0\,. \tag{2.39}$$

Next, by only considering the imaginary part in the beam parameter (we can assume the electric field is plane parallel in this case), the beam parameter becomes

$$\frac{1}{q(z)} = -i\frac{\lambda}{\pi w^2(z)}. \tag{2.40}$$

And, by inserting equation (2.40) into equation (2.39), we have

$$\frac{w^2(z)}{2}\frac{\partial^2}{\partial x^2}E_m(x) - 2x\frac{\partial}{\partial x}E_m(x) + ik\frac{w^2(z)}{2}\left[\frac{2}{A\left[q(z)\right]}\frac{d}{dq}A\left[q(z)\right] - \frac{1}{q(z)}\right]E_m(x) = 0. \tag{2.41}$$

Then, by substituting the variable with the relation $\sqrt{2}x/w(z) = u$, we finally obtain

$$\frac{\partial^2}{\partial u^2}E_m(u) - 2u\frac{\partial}{\partial u}E_m(u) + ik\frac{w^2(z)}{2}\left[\frac{2}{A\left[q(z)\right]}\frac{d}{dq}A\left[q(z)\right] - \frac{1}{q(z)}\right]E_m(u) = 0. \tag{2.42}$$

Note that equation (2.42) is similar to the differential equation for Hermite polynomials, $H_m(x)$.

$$\frac{d^2H_m(x)}{dx^2} - 2x\frac{dH_m(x)}{dx} + 2mH_m(x) = 0 \tag{2.43}$$

Thus, the electric field distribution has the form of a Hermite polynomial, i.e.,

$$E_m(x,z) = A\left[q(z)\right] \times H_m\left(\frac{\sqrt{2}x}{w(z)}\right) \times \exp\left[-ik\frac{x^2}{2q(z)}\right]. \tag{2.44}$$

In the same way, we can calculate the electric field distribution in the y-direction, and obtain the electric field distribution in the y-direction as

$$E_n(y,z) = A\left[q(z)\right] \times H_n\left(\frac{\sqrt{2}y}{w(z)}\right) \times \exp\left[-ik\frac{y^2}{2q(z)}\right]. \tag{2.45}$$

Thus, generally, the electric field distribution in the x- and y-directions is

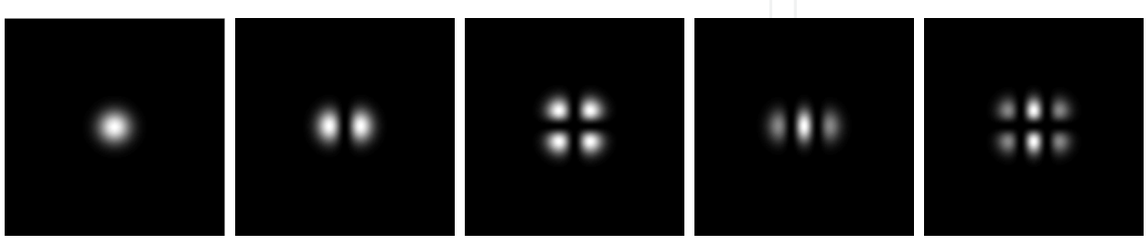

E_{00} E_{10} E_{11} E_{20} E_{21}

Fig. 1. Intensity distributions for several Hermite-Gaussian laser beam modes.

$$E_{mn}(x,y,z) = A\left[q(z)\right] \times H_m\left(\frac{\sqrt{2}x}{w(z)}\right) \times H_n\left(\frac{\sqrt{2}y}{w(z)}\right) \times \exp\left[-ik\frac{x^2+y^2}{2q(z)}\right], \tag{2.46}$$

though some Hermite polynomials of low order are given by

$$H_0(x) = 1,\ H_1(x) = x,\ H_2(x) = 4x^2 - 2, \text{ and } H_3(x) = 8x^3 - 12x. \tag{2.47}$$

Figure 1 shows some low order Hermite-Gaussian beam modes in the rectangular coordinate. The intensity distribution of the lowest beam mode ($m = n = 0$) is Gaussian and the Gaussian intensity profile is called either the TEM_{00} mode or the fundamental mode.

2.3 Laguerre-Gaussian beam mode in cylindrical coordinate

We can also solve the differential equation (2.16) in the cylindrical coordinate with a radially symmetric boundary condition. The solution of the wave equation in the cylindrical coordinates has the form of a Laguerre function; thus, the solution is called the Laguerre-Gaussian beam mode. In the cylindrical coordinates, the electric field propagating in the z-direction is given by

$$\frac{\partial^2 E(r,\phi,z)}{\partial r^2} + \frac{1}{r}\frac{\partial E(r,\phi,z)}{\partial r} + \frac{1}{r^2}\frac{\partial^2 E(r,\phi,z)}{\partial \phi^2} + \frac{\partial^2 E(r,\phi,z)}{\partial z^2} + k^2 E(r,\phi,z) = 0. \tag{2.48}$$

The solution for the differential equation (2.48) has the form of Laguerre polynomials. As such, the solution of the differential equation is given by

$$E_{mn}(r,\phi,z) = E_0\left(\frac{\sqrt{2}r(z)}{w(z)}\right)^n \times L_m^n\left(\frac{2r^2(z)}{w^2(z)}\right) \times \begin{Bmatrix}\cos(m\phi)\\ \sin(m\phi)\end{Bmatrix} \times \exp\left(-\frac{r^2(z)}{w^2(z)}\right). \tag{2.49}$$

Note that some low order Laguerre polynomials are given by

$$L_0^l(x) = 1,\ L_1^l(x) = l + 1 - x,\ L_2^l(x) = (l+1)(l+2)/2 - (l+2)x + x^2/2,$$

$$\text{and } L_3^l(x) = (l+1)(l+2)(l+3)/6 - (l+2)(l+3)x/2 + (l+3)x^2/2 - x^3/6. \tag{2.50}$$

Figure 2 shows some low order Laguerre-Gaussian beam modes in the cylindrical coordinate. Note that as for the Hermite-Gaussian beam, the lowest beam mode is Gaussian and is also called the fundamental mode.

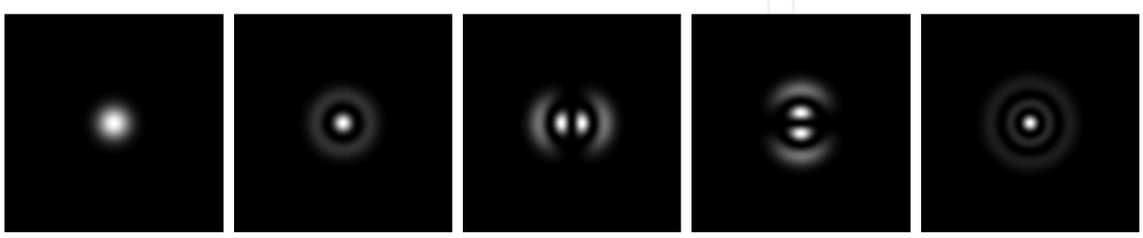

E_{00} E_{10} E_{11} (cos) E_{11} (sin) E_{20}

Fig. 2. Intensity distributions for several Laguerre-Gaussian laser beam modes.

2.4 Other beam modes

2.4.1. Flat-top beam profile and super Gaussian beam profile

In high-power laser systems, a uniform beam profile is required in order to efficiently extract energy from an amplifier. The uniform beam profile is sometimes called a flat-top (or top-hat) beam profile. However, the ideal flat-top beam profile is not possible because of diffraction; in many cases, a super-Gaussian beam profile is more realistic. The definition of the super-Gaussian beam profile is given by

$$\exp\left[-2r^{2n}/w_0^2\right]. \tag{2.51}$$

Here, n is called the order of the super-Gaussian beam mode and w_0 is the Gaussian beam radius when n is 1. Figure 3 shows the intensity profiles for several super-Gaussian beam profiles having different orders. As shown in the figure, the intensity profile becomes flat in the central region as the order of the super-Gaussian beam profile increases. Note that the flat-top beam profile is a specific case of the super-Gaussian beam profile having an order of infinity.

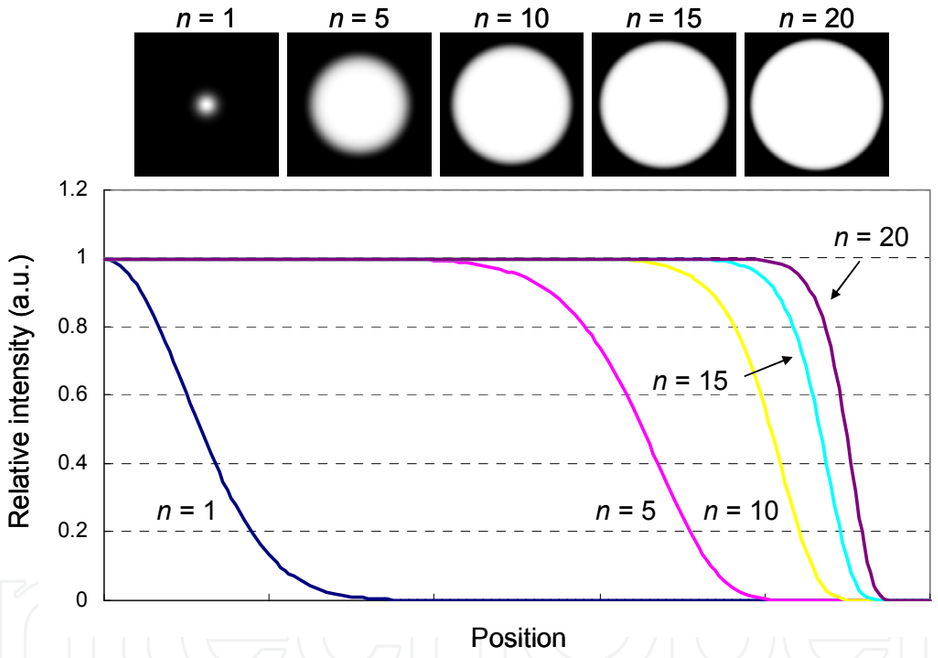

Fig. 3. Intensity distributions and their line profiles for several super-Gaussian laser beam modes having a different super-Gaussian order n.

2.4.2 Bessel-Gaussian beam profile

In this subsection, we will introduce a special laser beam mode called a Bessel beam. The Bessel function is a solution of the wave equation (2.16) in the cylindrical coordinate. Until 1987, the existence of the Bessel laser beam was not experimentally demonstrated. Theoretically, the Bessel laser beam has a special property that preserves its electric field distribution over a long distance. This is why the Bessel laser beam is referred to as a diffraction-free laser beam mode. However, in real situations, the Bessel laser beam mode preserves its electric field distribution for a certain distance because of the infinite power

problem. Now, let us derive the Bessel laser beam mode from the wave equation. The wave equation in the cylindrical coordinate can be rewritten as

$$\frac{\partial^2 E(r,\phi,z)}{\partial r^2}+\frac{1}{r}\frac{\partial E(r,\phi,z)}{\partial r}+\frac{1}{r^2}\frac{\partial^2 E(r,\phi,z)}{\partial \phi^2}+\frac{\partial^2 E(r,\phi,z)}{\partial z^2}+k^2 E(r,\phi,z)=0\,. \tag{2.48}$$

Then, using the separation of variables, the solution for equation (2.48) is

$$E(r,\phi,z)=E(r,\phi)\times\exp(-i\beta z)\,, \tag{2.52}$$

and by inserting equation (2.52) into equation (2.48), equation (2.48) becomes

$$\frac{\partial^2 E(r,\phi,z)}{\partial r^2}+\frac{1}{r}\frac{\partial E(r,\phi,z)}{\partial r}+\frac{1}{r^2}\frac{\partial^2 E(r,\phi,z)}{\partial \phi^2}+\left(k^2-\beta^2\right)E(r,\phi,z)=0\,. \tag{2.53}$$

If the electric field is radially symmetric, then the electric field $E(r,\phi,z)$ becomes $E(r,z)$ and the derivative with respect to the angular direction vanishes, i.e.,

$$r^2\frac{\partial^2 E(r,z)}{\partial r^2}+r\frac{\partial E(r,z)}{\partial r}+\left(k^2-\beta^2\right)r^2E(r,z)=0\,. \tag{2.54}$$

Note that equation (2.54) is similar to Bessel's differential equation with an order of 0. The Bessel's differential equation is expressed as

$$\rho^2\frac{d^2}{d\rho^2}Z_v(k\rho)+\rho\frac{d}{d\rho}Z_v(k\rho)+\left(k^2\rho^2-v^2\right)Z_v(k\rho)=0\,. \tag{2.55}$$

And, the solution of equation (2.54) is given by

$$E(r,z)=E_0\times J_0\left(\sqrt{k^2-\beta^2}\,r\right)\times\exp(-i\beta z)\,. \tag{2.56}$$

Thus, the solution in the cylindrical coordinate for the differential equation for the electric field is shown to be the Bessel function. Figure 4 presents the intensity distribution and profile for the Bessel laser beam mode.

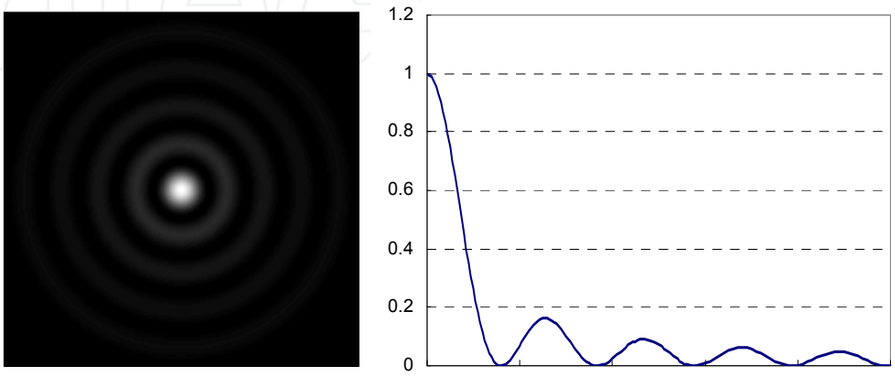

Fig. 4. Intensity distribution and its line profile for Bessel laser beam mode.

In 1987, Gori *et al.* introduced the Bessel-Gaussian laser beam mode to avoid the infinite power problem. In the Bessel-Gaussian laser beam mode, the electric field is given by

$$E(r,z_0)=E_0\times J_0(\beta r)\times\exp\left(-\frac{r^2(z_0)}{w^2(z_0)}\right). \tag{2.57}$$

3. Intensity distribution of the focused laser beam

In the previous section, we derived the electric field distribution referred to as the laser beam mode. In order to determine the beam quality (or propagation) factor for the laser beam mode, we need to know the focusing property of the laser beam. The electric field distribution of a focused laser beam can be theoretically calculated from an incident beam profile. In this section, the calculation of the electric field distribution of a focused laser beam is introduced. For this task, three different approaches are used: a geometrical approach using a ray transfer matrix, a wave optics approach using diffraction theory, and a Fourier transform approach. From the geometrical approach, the physical insight and useful relationships for Gaussian beam parameters before and after a focusing optic can be easily obtained. However, if the incident beam profile is not Gaussian and has a wavefront aberration, it becomes more difficult to use the geometrical approach to explain the focusing property of the laser beam. In this case, the wave optics approach using diffraction theory gives more accurate calculation results. The wave optics approach offers analytic solutions for a Gaussian and uniform laser beams. However, the wave optics approach does not provide an analytical solution for an arbitrary incident laser beam mode. In this case, the Fourier transform approach becomes very useful. By using the Fourier transform method, the electric field distribution of the focused laser beam can be easily obtained and, together with the focus shift method, the electric field distribution near the focal plane can be quickly obtained. In particular, the Fourier transform approach is more useful for a laser beam having a wavefront aberration.

3.1 Geometrical approach

Propagation of the electric field can be described by the ray transfer matrix of an optical element. The ray transfer matrix determines the deviation angle at a location of the optical element; this matrix is also called the ABCD matrix and is expressed by

$$\begin{bmatrix} A & B \\ C & D \end{bmatrix}. \tag{3.1}$$

Let us now consider the case in which a Gaussian laser beam passes through an optical element having ABCD elements. The Gaussian beam mode [$E_1(x_1,y_1,z_1)$] before the optical element is again

$$E_1(x_1,y_1,z_1)=A(z_1)\times\exp\left[-ik\frac{x_1^2+y_1^2}{2q(z_1)}\right] \text{ and } \frac{1}{q(z_1)}=\frac{1}{R(z_1)}-i\frac{\lambda}{\pi w_1^2(z_1)}. \tag{3.2}$$

Then, when the Gaussian laser beam passes through the optical element, the electric field right after the optical element is determined by

$$E_2(x_2,z_1) \sim A(z_1)\int \exp\left[-\frac{ik}{2q(z_1)}x_1^2\right]\exp\left[-i\frac{\pi}{\lambda B}\left(Ax_1^2+Dx_2^2-2x_1x_2\right)\right]dx_1$$
$$= A(z_1)\int \exp\left[-\left(\frac{ik}{2q(z_1)}+\frac{i\pi}{\lambda B}A\right)x_1^2 - i\frac{\pi}{\lambda B}Dx_2^2 + 2i\frac{\pi}{\lambda B}x_1x_2\right]dx_1 \quad . \tag{3.3}$$

Here, only the electric field in the x-direction is considered, though the electric field in the y-direction can be calculated in the same manner. After some calculation, the electric field after the optical element is given by

$$E_2(x_2) = \sqrt{\frac{\pi}{\frac{ik}{2q_1}+\frac{i\pi}{\lambda B}A}}\exp\left[\frac{ik}{2B}x_2^2\left(-D+\frac{1}{B/q_1+A}\right)\right]. \tag{3.4}$$

The following definite integral formula (3.5) is used to derive equation (3.4).

$$\int_{-\infty}^{\infty}\exp\left(-ax^2-2bx\right)dx = \sqrt{\frac{\pi}{a}}\exp\left(\frac{b^2}{a}\right). \tag{3.5}$$

Because the determinant of the matrix is 1 (i.e., $AD-BC=1$), the electric field distribution after the optical element can be rewritten as follows:

$$E_2(x_2) = \sqrt{\frac{\pi}{\frac{ik}{2q_1}+\frac{i\pi}{\lambda B}A}}\exp\left[-\frac{ik}{2}x_2^2\left(\frac{q_1C+D}{q_1A+B}\right)\right]. \tag{3.6}$$

By defining $\frac{1}{q_2}$ as $\frac{q_1C+D}{q_1A+B}$, the resultant electric field distribution again has the same expression as the incident electric field except for the laser beam parameter q_2, such that

$$E_2(x_2) \sim \exp\left[-\frac{ik}{2q_2}x_2^2\right]. \tag{3.7}$$

Again, let us assume the Gaussian laser beam is focused by a focusing optic having a focal length of f. Then, we need to determine the electric field distribution at the focal plane of the focusing optic; the ray transfer matrix for a focusing optic and a free distance is given by

$$\begin{bmatrix} A & B \\ C & D \end{bmatrix} = \begin{bmatrix} 1 & f \\ 0 & 1 \end{bmatrix}\begin{bmatrix} 1 & 0 \\ -1/f & 1 \end{bmatrix} = \begin{bmatrix} 0 & f \\ -1/f & 1 \end{bmatrix}. \tag{3.8}$$

If the incident Gaussian laser beam is an ideal plane wave (i.e. $R(z_1)=\infty$), $q(z_1)$ is simply defined as $i\frac{\pi w_1^2(z_1)}{\lambda}$. Then, $\frac{1}{q_2}$ can be quickly calculated as

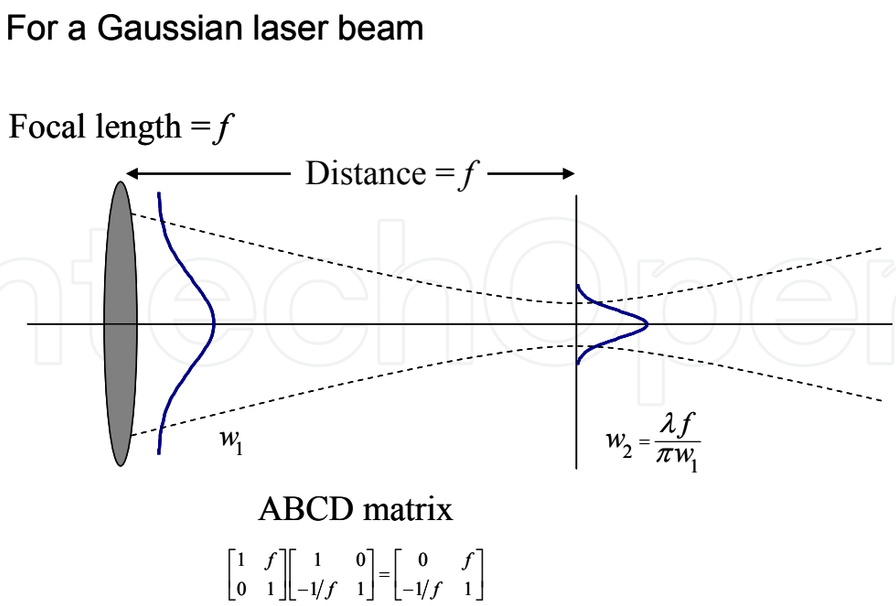

Fig. 5. Focusing Gaussian laser beam mode having a focusing optic with a focal length of f .

$$\frac{1}{q_2} = \frac{1}{R_2} - i\frac{\lambda}{\pi w_2^2} = -i\frac{\pi w_1^2}{\lambda}\frac{1}{f^2} + \frac{1}{f}\,. \tag{3.9}$$

Thus, the intensity profile of a focused Gaussian beam is again Gaussian with a new Gaussian width w_2 , which is given by

$$w_2 = \frac{\lambda f}{\pi w_1} = \frac{w_1 f}{z_R^2}\,, \tag{3.10}$$

where z_R is defined as $w_2 = \dfrac{\lambda f}{\pi w_1} = \dfrac{w_1 f}{z_R^2}$ and called the Rayleigh range, at which point the area of the laser beam increases by a factor of 2. The electric field distribution near the focal plane can be calculated by replacing the focal length f with the distance d in equation (3.8). However, even if an arbitrary optical element having an arbitrary wavefront aberration can be represented by a ray transfer matrix, the general description of the electric field distribution for an arbitrary electric field cannot be simply expressed by the geometrical approach.

3.2 Wave optics approach using diffraction theory

Now, in this section, we will directly calculate the electric field distribution based on the diffraction integral. Again, consider that an electric field converges from a focusing optic having a focal length of f to the axial focal point. Then, the electric field distribution at a point (x_2, y_2) in the focal plane is given by

$$E(x_2, y_2) = -\frac{i}{\lambda}\frac{e^{-ikf}}{f}\int E_1(x_1, y_1)\frac{e^{iks}}{s}dx_1 dy_1\,. \tag{3.11}$$

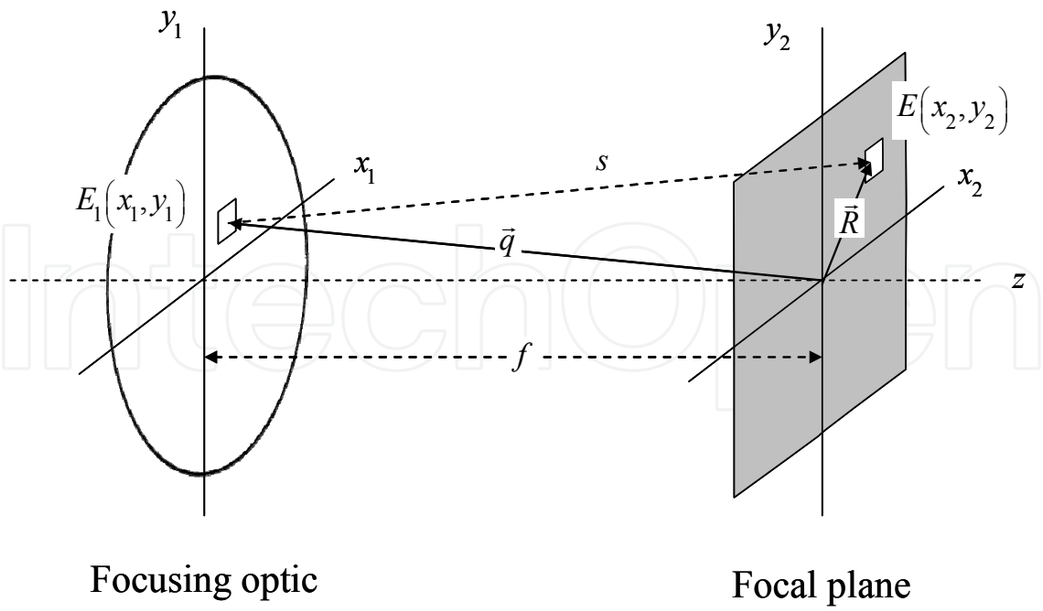

Fig. 6. Diffraction of electric field at a focusing optic having a focal length f.

To evaluate equation (3.11), let us assume that the focusing optic is circular and that the radius of the focusing optic is a. Then, it is convenient to express (x_1, y_1, z_1) and (x_2, y_2, z_2) in the cylindrical coordinate as follows:

$$x_1 = a\rho\sin\theta,\ y_1 = a\rho\cos\theta, \text{ and } x_2 = r\sin\varphi,\ y_2 = r\cos\varphi \tag{3.12}$$

where ρ extends from zero to 1. In this expression, from Fig. 6, the difference $s - f$ and the small area of $dx_1 dy_1$ can be, via an approximation, expressed as

$$s - f = -\vec{q}\cdot\vec{R} \text{ and } dx_1 dy_1 = f^2 d\Omega \tag{3.13}$$

where $d\Omega$ is the infinitesimal solid angle. Then, using the approximation $s \approx f$, the electric field distribution at a point (x_2, y_2) becomes

$$E(x_2, y_2) = -\frac{i}{\lambda}\int E_1(x_1, y_1) e^{-ik\vec{q}\cdot\vec{R}} d\Omega\,. \tag{3.14}$$

Equation (3.14) is known as the Debye integral and expresses the electric field as a superposition of plane wave components having different directions of propagation, known as angular spectrums. The phase component in the integral is

$$\vec{q}\cdot\vec{R} = \frac{x_1x_2 + y_1y_2 + z_1z_2}{f}, \tag{3.15}$$

and the axial position z_1 of element $dx_1 dy_1$ from the origin of (x_2, y_2, z_2) is

$$z_1 = -\sqrt{f^2 - a^2\rho^2} = -f\left[1 - \frac{1}{2}\frac{a^2\rho^2}{f^2} + \frac{3}{8}\frac{a^4\rho^4}{f^4} - \cdots\right]. \tag{3.16}$$

By inserting equation (3.16) into equation (3.15) and using $f \gg a$, we obtain the following expression for the phase component in the Debye integral:

$$k\vec{q}\cdot\vec{R} = k\frac{x_1x_2 + y_1y_2 + z_1z_2}{f} = \frac{2\pi}{\lambda}\frac{a\rho r\cos(\theta-\varphi)}{f} - z\frac{2\pi}{\lambda}\left[1-\frac{1}{2}\frac{a^2\rho^2}{f^2}\right]. \tag{3.17}$$

Then, by introducing dimensionless variables u and v in the focal plane, defined as

$$u = \frac{2\pi}{\lambda}\left(\frac{a}{f}\right)^2 z \text{ and } v = \frac{2\pi}{\lambda}\left(\frac{a}{f}\right)r, \tag{3.18}$$

the phase component in the Debye integral is

$$k\vec{q}\cdot\vec{R} = v\rho\cos(\theta-\varphi) - \left(\frac{f}{a}\right)^2 u + \frac{1}{2}u\rho^2. \tag{3.19}$$

Thus, equation (3.14), which expresses the electric field distribution in the focal plane, becomes

$$E(u,v) = -\frac{i}{\lambda}\frac{a^2}{f^2}\exp\left[i\left(\frac{f}{a}\right)^2 u\right]\int_0^1\int_0^{2\pi} E(\rho,\theta)\exp\left\{-i\left[v\rho\cos(\theta-\varphi)+\frac{1}{2}u\rho^2\right]\right\}\rho d\rho d\theta \,. \tag{3.20}$$

And, if the incoming electric field is radially symmetric, equation (3.20) can be simply expressed as

$$E(u,v) = -\frac{2\pi i}{\lambda}\frac{a^2}{f^2}\exp\left[i\left(\frac{f}{a}\right)^2 u\right]\int_0^1 E(\rho)J_0(v\rho)\exp\left[-i\frac{1}{2}u\rho^2\right]\rho d\rho\,, \tag{3.21}$$

using the definition of Bessel function.

$$J_0(x) = \frac{1}{2\pi}\int_0^{2\pi}\exp(ix\cos\theta)d\theta\,. \tag{3.22}$$

If we consider the uniform intensity profile, then the incoming electric field is constant with respect to the position (i.e. $E(\rho,\theta) = C$). In this case, the electric field distribution in the focal plane has the form

$$E(u,v) = -i\frac{2\pi}{\lambda}\frac{a^2C}{f^2}\exp\left[i\left(\frac{f}{a}\right)^2 u\right]\int_0^1 J_0(v\rho)\exp\left(-\frac{1}{2}iu\rho^2\right)\rho d\rho\,. \tag{3.23}$$

To calculate equation (3.35) further, we separate the integral into the real and imaginary parts.

$$E(u,v) = -i\frac{2\pi}{\lambda}\frac{a^2C}{f^2}\exp\left[i\left(\frac{f}{a}\right)^2 u\right]\left[\int_0^1 J_0(v\rho)\cos\left(\frac{1}{2}u\rho^2\right)\rho d\rho - i\int_0^1 J_0(v\rho)\sin\left(\frac{1}{2}u\rho^2\right)\rho d\rho\right]. \tag{3.24}$$

There are two different cases in evaluating the integrals in equation (3.24). In the first case, when $|u/v|<1$ (i.e. inside the geometrical shadow), we use the relation for the Bessel function to obtain

$$2\int_0^1 J_0(v\rho)\cos\left(\frac{1}{2}u\rho^2\right)\rho d\rho = \frac{2}{v}\int_0^1 \frac{d}{d\rho}\left[\rho J_1(v\rho)\right]\cos\left(\frac{1}{2}u\rho^2\right)\rho d\rho$$

$$\begin{aligned}
&= \frac{2}{v}\left[J_1(v)\cos\left(\frac{1}{2}u\right) + u\int_0^1 \rho^2 J_1(v\rho)\sin\left(\frac{1}{2}u\rho^2\right)\rho d\rho\right] \\
&= \frac{\cos(u/2)}{u/2}\left[\left(\frac{u}{v}\right)J_1(v) - \left(\frac{u}{v}\right)^3 J_3(v) + \cdots\right] + \frac{\sin(u/2)}{u/2}\left[\left(\frac{u}{v}\right)^2 J_2(v) - \left(\frac{u}{v}\right)^4 J_4(v) + \cdots\right]. \quad (3.25) \\
&= \frac{\cos(u/2)}{u/2}U_1(u,v) + \frac{\sin(u/2)}{u/2}U_2(u,v)
\end{aligned}$$

where the following definition of the Lommel function $U_n(u,v)$ and the relation for the Bessel function are used to obtain equation (3.25):

$$U_n(u,v) = \sum_{s=0}^{\infty}(-1)^s\left(\frac{u}{v}\right)^{n+2s} J_{n+2s}(v), \quad (3.26)$$

$$\text{and } \frac{d}{dx}\left[x^{n+1}J_{n+1}(x)\right] = x^{n+1}J_n(x). \quad (3.27)$$

In a similar way, we obtain the expression for the imaginary part:

$$2\int_0^1 J_0(v\rho)\sin\left(\frac{1}{2}u\rho^2\right)\rho d\rho = \frac{\sin(u/2)}{u/2}U_1(u,v) - \frac{\cos(u/2)}{u/2}U_2(u,v). \quad (3.28)$$

In the second case, when $|u/v|>1$ (i.e. outside the geometrical shadow), we evaluate equation (3.24) by integrating by parts with respect to the trigonometric function in order to finally obtain the expressions for the real and imaginary parts as follows:

$$2\int_0^1 J_0(v\rho)\cos\left(\frac{1}{2}u\rho^2\right)\rho d\rho = \frac{\sin\left(v^2/2u\right)}{u/2} + \frac{\sin(u/2)}{u/2}V_0(u,v) - \frac{\cos(u/2)}{u/2}V_1(u,v), \quad (3.29)$$

$$\text{and} \quad 2\int_0^1 J_0(v\rho)\sin\left(\frac{1}{2}u\rho^2\right)\rho d\rho = \frac{\cos\left(v^2/2u\right)}{u/2} - \frac{\cos(u/2)}{u/2}V_0(u,v) - \frac{\sin(u/2)}{u/2}V_1(u,v). \quad (3.30)$$

The other definition of the Lommel function, $V_n(u,v)$, is then used for obtaining equations (3.29) and (3.30).

$$V_n(u,v) = \sum_{s=0}^{\infty}(-1)^s\left(\frac{v}{u}\right)^{n+2s} J_{n+2s}(v). \quad (3.31)$$

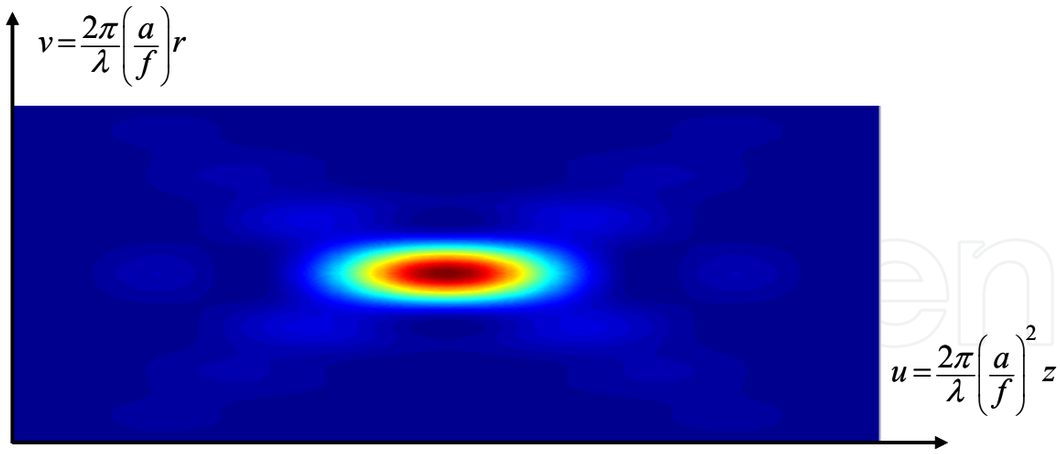

Fig. 7. Intensity distribution near the focal plane calculated using the diffraction integral approach when a flat-top beam profile is focused.

Now, let us calculate the electric field distribution in the focal plane from equations (3.21), (3.25), (3.28), (3.29), and (3.30). First, in the region $|u/v|<1$, we use equations (3.21), (3.25), and (3.28) to calculate the intensity distribution.

$$I(u,v)=4I_0\left[\frac{U_1^2(u,v)+U_2^2(u,v)}{u^2}\right]. \tag{3.32}$$

Figure 7 shows the intensity distribution near the focal plane calculated using equation (3.32) when a flap-top laser beam is focused. In the special case of a focal plane ($u=0$), the intensity distribution is

$$I(0,v)=4I_0\frac{J_1^2(v)}{v^2}. \tag{3.33}$$

Thus, as shown in equation (3.33), the Airy function is obtained when we focus a uniform electric field. If the incoming laser beam has a Gaussian beam profile, then the electric field distribution in equation (3.21) has the form

$$E_1(\rho)=C\times\exp\left[-\frac{a^2\rho^2}{w_0^2}\right]. \tag{3.34}$$

In equation (3.34), we only consider the case of a plane wave (i.e. $R=\infty$). By inserting equation (3.34) into equation (3.21), equation (3.21) becomes

$$\begin{aligned}E(u,v)&=-\frac{2\pi i}{\lambda}\frac{a^2C}{f^2}\exp\left[i\left(\frac{f}{a}\right)^2u\right]\int_0^1\exp\left[-\frac{a^2\rho^2}{w_0^2}\right]J_0(v\rho)\exp\left[-i\frac{1}{2}u\rho^2\right]\rho d\rho\\&\approx\int_0^1 J_0(v\rho)\exp\left[-\left(\frac{a^2}{w_0^2}+i\frac{u}{2}\right)\rho^2\right]\rho d\rho\end{aligned}. \tag{3.35}$$

Again, in the special case of a focal plane ($u=0$), the electric field distribution in the focal plane is

$$E(0,v) \approx \int_0^1 J_0(v\rho)\exp\left(-\frac{a^2\rho^2}{w_0^2}\right)\rho d\rho \,. \tag{3.36}$$

To integrate equation (3.36), we use the following definite integral formula:

$$\int_0^\infty \exp\left(-\alpha x^2\right) I_m(\beta x) J_m(\gamma x) x dx = \frac{1}{2\alpha}\exp\left(\frac{\beta^2-\gamma^2}{4\alpha}\right) J_m\left(\frac{\beta\gamma}{2\alpha}\right). \tag{3.37}$$

The small beam size approximation ($a \gg w_0$) is used to apply the definite integral formula. Then, the final expression for the incoming Gaussian beam is

$$E(0,v) \approx \int_0^1 J_0(v\rho)\exp\left(-\frac{a^2\rho^2}{w_0^2}\right)\rho d\rho = \frac{w_0^2}{2a^2}\exp\left(-\frac{w_0^2 v^2}{4a^2}\right) = \frac{w_0^2}{2a^2}\exp\left(-\frac{r^2}{w_1^2}\right). \tag{3.38}$$

From equation (3.38), the new Gaussian beam size for the focused electric field is obtained as

$$w_1 = \frac{\lambda f}{\pi w_0} \,. \tag{3.39}$$

Obviously, the new Gaussian beam size for the focused electric field calculated from the Debye integral is exactly the same as that calculated from the geometrical approach. Unlike the above special cases (uniform and Gaussian field profiles), an analytical solution for the

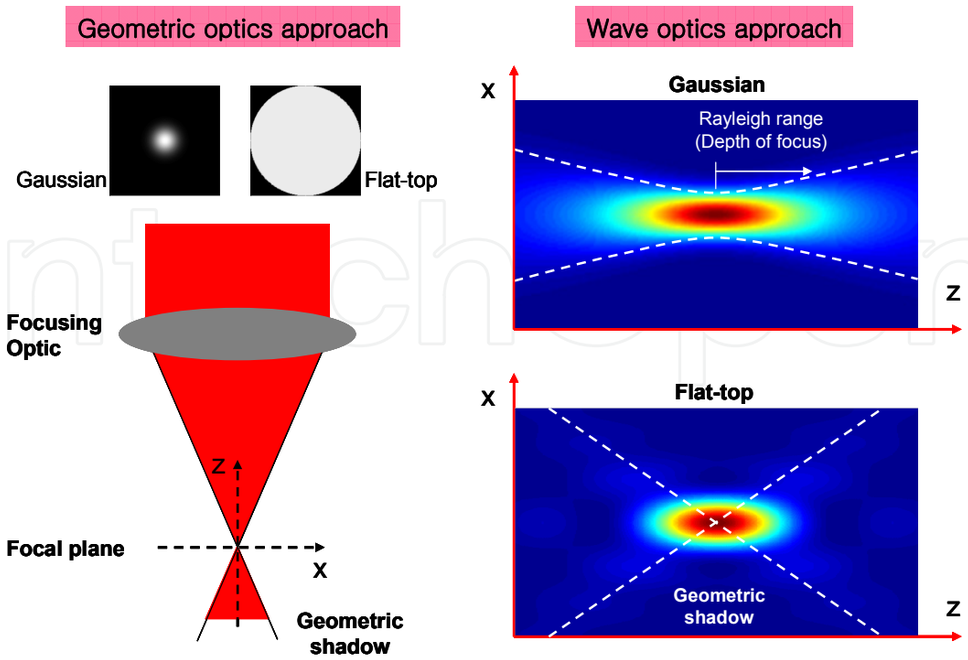

Fig. 8. Focusing laser beam: geometrical optics and wave optics approaches.

focused electric field does not exist for an electric field having an arbitrary magnitude and wavefront. Thus, in case of an arbitrary electric field, it is convenient to use the Fourier transform approach to calculate the focused electric or intensity distribution in and near the focal plane.

3.3 Fourier transform approach

If we assume that a laser beam is focused with an ideal focusing optic having a focal length f, then the electric field distribution at the focal plane can be expressed by

$$E_2(x_2,y_2) \sim \int_{-\infty}^{\infty} E_1(x_1,y_1)\exp\left[ikW(x_1,y_1)\right]\exp\left[i\frac{k}{f}(x_1x_2+y_1y_2)\right]dx_1dy_1 . \tag{3.40}$$

This integral form represents the Fourier transform of the incident electric field having an arbitrary wavefront aberration $W(x_1,y_1)$. Now, let us quickly review the derivation of equation (3.40). Consider that a monochromatic electric field $E_1(x_1,y_1)$ converges by a focusing optic having a focal length f to the axial focal point. Again, the electric field distribution at a point (x_2, y_2) in the focal plane is given by

$$E(x_2,y_2) = -\frac{i}{\lambda}\frac{e^{-ikf}}{f}\int E_1(x_1,y_1)\frac{e^{iks}}{s}dx_1dy_1 \tag{3.11}$$

where x_1 and y_1 are the coordinates in the aperture plane, and s is the distance from a certain point in the focusing optic to the point (x_2, y_2). Then, if we express s in the (x, y) coordinate, s is

$$\begin{aligned} s &= \sqrt{(x_1-x_2)^2+(y_1-y_2)^2+z_2^2} = z_2\sqrt{1+\left(\frac{x_1-x_2}{z_2}\right)^2+\left(\frac{y_1-y_2}{z_2}\right)^2} \\ &\approx z_2\left[1+\frac{1}{2}\left(\frac{x_1-x_2}{z_2}\right)^2+\frac{1}{2}\left(\frac{y_1-y_2}{z_2}\right)^2\right] \end{aligned} . \tag{3.41}$$

Because the phase of the electric field varies more quickly than the magnitude, we can approximate s such that $s \approx z_2 \approx f$ in the expression related to the magnitude. Thus, equation (3.11) becomes

$$E(x_2,y_2) = -\frac{i}{\lambda}\frac{e^{-ikf}}{f^2}\exp\left[\frac{ik}{2f}\left(x_2^2+y_2^2\right)\right]\int E_1(x_1,y_1)\exp\left[\frac{ik}{2f}\left(x_1^2+y_1^2\right)\right]\exp\left[-\frac{k}{f}(x_1x_2+y_1y_2)\right]dx_1dy_1 . \tag{3.42}$$

We then derive the expression for electric field distribution in a focal plane when the electric field is focused with a focusing optic having a focal length f. In equation (3.42), one important consideration is the phase delay due to the focusing optic; the phase function including phase delay should be considered in the electric field $E_1(x_1,y_1)$. For this task, we first have to obtain the expression for the phase delay. If we consider a lens having the thickness shown in Fig. 9, then the phase delay after the lens is

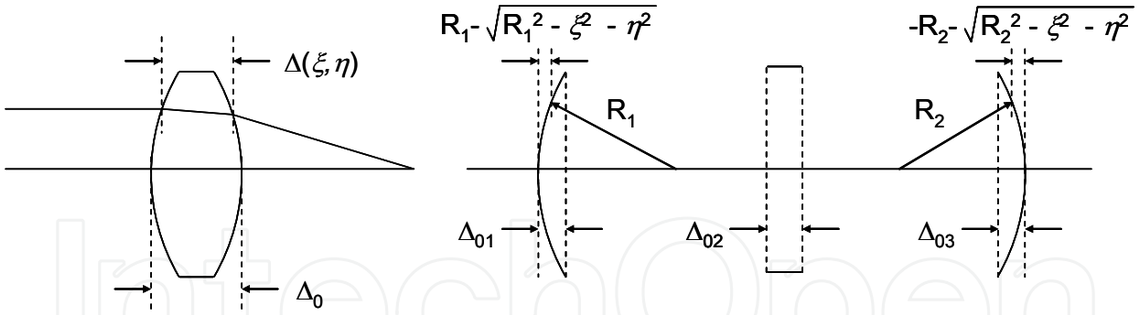

Fi. 9. Calculation of lens thickness function for inducing the phase delay.

$$\phi(x_1, y_1) = nkT(x_1, y_1) + k\left[T_0 - T(x_1, y_1)\right] \tag{3.43}$$

where n is the refractive index of the lens, T_0 is the center thickness of the lens, and $T(x_1, y_1)$ is the thickness function of the lens at a position (x_1, y_1). By considering the geometry of the lens in Fig. 9, the thickness function $T(x_1, y_1)$ can be written as

$$T(x_1, y_1) = T_0 - R_1\left(1 - \sqrt{1 - \frac{x_1^2 + y_1^2}{R_1^2}}\right) + R_2\left(1 - \sqrt{1 - \frac{x_1^2 + y_1^2}{R_2^2}}\right). \tag{3.44}$$

Then, by using a paraxial approximation, we can take only the first two terms in the Taylor series of $\sqrt{\ }$. The thickness function can be simply rewritten as

$$T(x_1, y_1) = T_0 - \frac{x_1^2 + y_1^2}{2}\left(\frac{1}{R_1} - \frac{1}{R_2}\right). \tag{3.45}$$

From equation (3.45), the phase function $P(x_1, y_1)$ after a thin lens is

$$P(x_1, y_1) = \exp\left[-i\phi(x_1, y_1)\right] = \exp\left[-i\frac{k}{2f}\left(x_1^2 + y_1^2\right)\right]. \tag{3.46}$$

Note that the mathematical formula (3.47) for a lens having radii R_1 and R_2 is used to derive equation (3.46).

$$\frac{1}{f} = (n-1)\left(\frac{1}{R_1} - \frac{1}{R_2}\right). \tag{3.47}$$

Thus, the final expression for the electric field $E_1(x_1, y_1)$ after the lens is

$$E_1(x_1, y_1) = E_0(x_1, y_1)\exp\left[-i\frac{k}{2f}\left(x_1^2 + y_1^2\right)\right] \tag{3.48}$$

where $E_1(x_1, y_1)$ means the electric field before the focusing optic. By substituting equation (3.48) into equation (3.42), we quickly obtain equation (3.40). By the same analogy used in equation (3.48), the expression for the wavefront aberration is introduced in equation (3.40).

From equation (3.40), in order to obtain the electric field distribution at the focal plane, an accurate measurement of the wavefront aberration is required.

The wavefront aberration means the deviation of the spatial phase of the laser beam from the reference phase, typically due to imperfections in optics used in the laser system and the beam delivery line and the thermal property of the laser crystal. The wavefront aberration, especially higher-order aberrations, is usually negligible in a small laser system. However, as the size of the laser system (specifically, the beam size) becomes larger, the wavefront aberration of the laser beam can no longer be considered negligible. The wavefront aberration can be expressed using Zernike polynomials $Z_n^m(x,y)$ as follows:

$$W(x,y) = \sum_{n,m} c_{nm} Z_n^m(x,y) \tag{3.49}$$

where n and m are the radial and azimuthal order for the Zernike polynomial, and c_{nm} is the Zernike coefficient. A double-index scheme in the OSA/ANSI standard is generally used to label the Zernike coefficients.

The Shack-Hartmann wavefront sensor is commonly used to measure the wavefront aberration. Figure 10 presents a typical schematic diagram of a Shack-Hartmann wavefront sensor, which consists of a microlens array and a CCD camera. The size of the microlens array ranges from about 100 μm to several hundreds of μm. The microlens array divides the laser beam into hundreds of sub-apertures and focuses them onto the CCD camera. The CCD camera then records the focal spots formed by the microlens array. Next, the locations of focal spots are calculated and compared to the reference position, i.e., when the laser beam has no wavefront aberration. Here, deviations from the reference positions provide the wavefront information. Once the wavefront aberration is obtained, the electric field distribution in the focal plane can be quickly calculated using equation (3.40).

Many other techniques, such as the interferometric method, have been devised to measure the wavefront of the laser beam. Figure 11 describes how to measure the wavefront aberration of a laser beam using a shearing interferometer. Also, the wavefront aberration

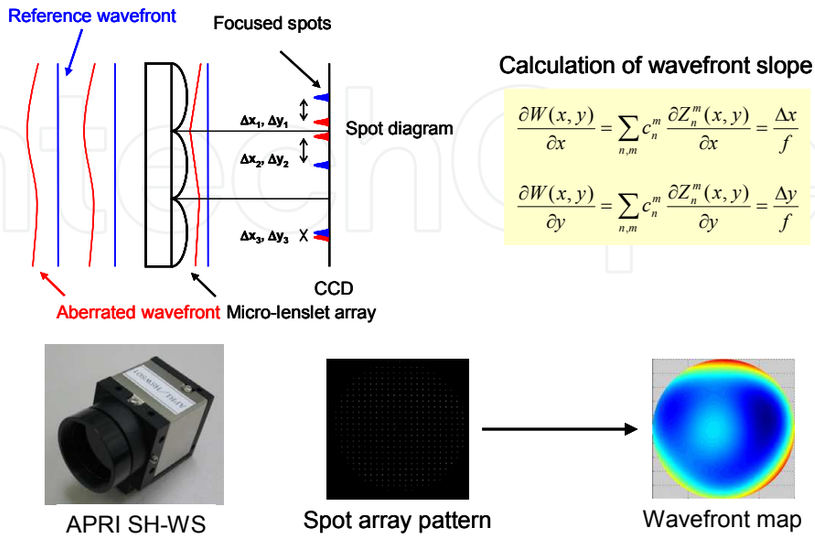

Fig. 10. Principle of Shack-Hartmann wavefront sensing.

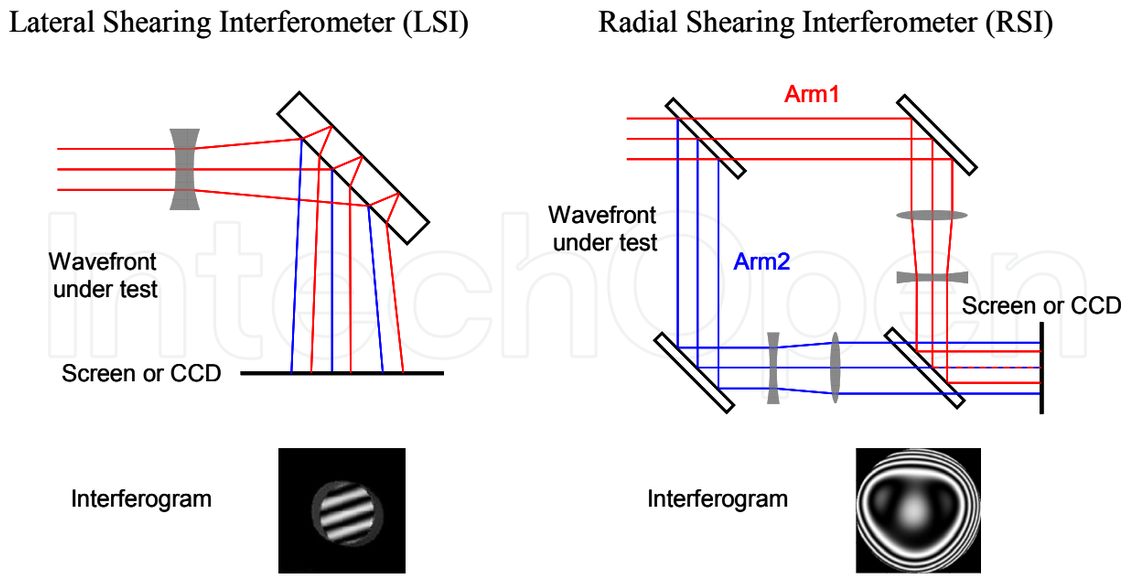

Fig. 11. Lateral and radial shearing interferometers for measuring wavefront of laser beam.

can be reconstructed by directly measuring the focal spot. This technique is called phase retrieval technique. However, the use of this technique is quite limited because the wavefront reconstruction takes time due to the iteration process.

Because the Fourier transform only offers the electric field distribution in the focal plane, a special technique called the focus-shift technique is required in order to calculate the electric field distribution near the focal plane. Figure 12 explains the principle of focus-shift technique. In the figure, if an incident laser beam has no wavefront aberration, the laser beam is then focused at the focal plane of a focusing optic having a focal length of f. If a certain amount (c_{20}) of defocus is intentionally added to the wavefront aberration of the laser beam, the laser beam itself will converge and the focal spot will instead be formed at position d, given by

$$\frac{1}{d} = \frac{4\sqrt{3}c_{20}}{r_0^2} \tag{3.50}$$

where c_{20} is the Zernike coefficient for defocus, and r_0 is the radius of the laser beam. Thus, the added defocus will act as a virtual focusing optic having a focal length of d. Again, if the defocused laser beam is focused by the focusing optic, a new focus will form at position d_{new} due to the dioptric law, such that (see Fig. 12(b)):

$$\frac{1}{d_{new}} = \frac{1}{f} + \frac{1}{d} = \frac{1}{f} + \frac{4\sqrt{3}c_{20}}{r_0^2}. \tag{3.51}$$

According to Eq. (3.51), the position of the laser focal spot can be accurately controlled by adding a proper amount of defocus to the wavefront of the incoming laser beam. As mentioned above, this technique is useful in calculating the intensity distribution near the focal plane. Because the Fourier transform of a laser beam always provides the intensity

distribution in the focal plane of a focusing optic, the intensity distribution calculated with a different amount of defocus value expresses the intensity distribution of the original laser beam in the plane of z (Fig. 12(b)). In the figure, z is defined by $f - d_{new}$; thus, by introducing various amounts of defocus to the wavefront of an incoming laser beam and performing a finite Fourier transform (FFT), a full description of the three-dimensional intensity distribution near the focal plane is possible for an arbitrary laser beam without having to calculate the diffraction integral in equation (3.11). Of course, the focus-shift technique holds under the thin-lens approximation and under the condition of adding a small amount of defocus. Figure 13 shows the intensity distribution near the focal plane calculated using the Fourier transform approach when a flat-top laser beam profile is focused. As shown in the figure, the overall intensity profile is almost identical to that calculated with the wave optics approach. Also, the Fourier transform approach can be applied to quickly calculate the intensity distribution of a laser pulse near the focal plane.

In order to calculate the intensity distribution of a laser pulse (especially for an ultrashort laser pulse in the femtosecond regime), we have to consider chromatic aberration induced by a focusing optic. The chromatic aberration means the change in defocus values at different wavelengths. Figure 14 shows the calculated and the measured defocus values (c_{20} s), as functions of wavelength, that were induced by the beam expanders in a high power Ti:sapphire laser system. Here, ray-tracing software was used to calculate c_{20} s for the beam expanders at different wavelengths, the values of which are seen to almost linearly

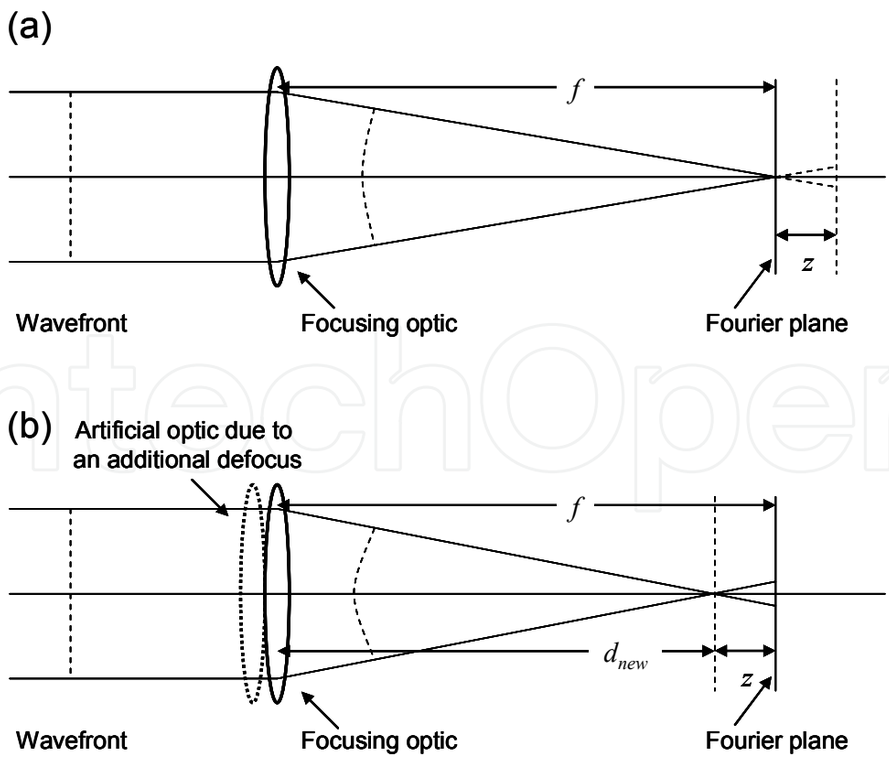

Fig. 12. Explanation of focus-shift technique introducing an arbitrary defocus into laser beam.

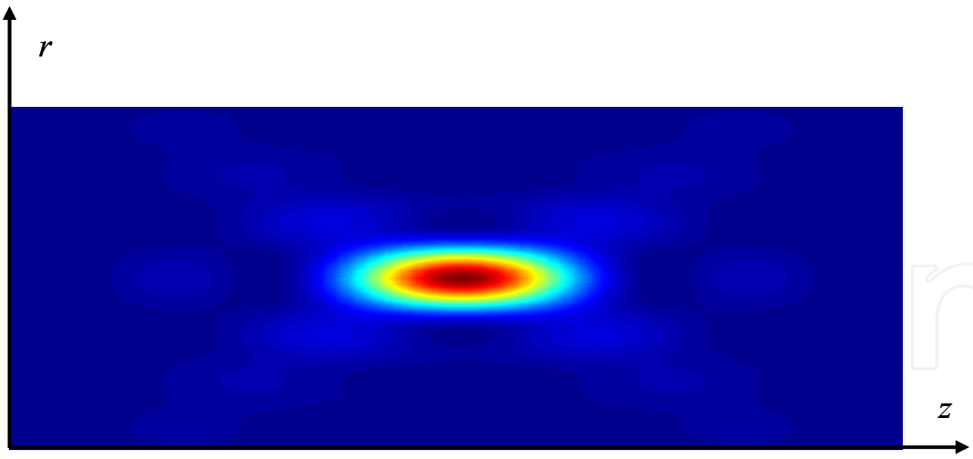

Fig. 13. Intensity distribution near the focal plane calculated using the Fourier transform approach when a flat-top beam profile is focused.

decrease with increasing wavelengths. This decrease implies that, after the beam expanders, the short-wavelength component in the laser spectrum converges while the long-wavelength component diverges. The slope of the decrease was 0.058 μm/10 nm. The change in defocus of the laser pulse in the spectral range was then measured to investigate the chromatic aberration caused by the beam expanders. A wavefront sensor was used to measure the defocus values of the laser pulse at different wavelengths.

Bandpass filters having a bandwidth of 10 nm at wavelengths of 760, 780, 800, 820, and 840 nm, respectively, were placed in front of the wavefront sensor to examine the dependence of the defocus value on the wavelength. The squares in Fig. 14 indicate the measured defocus values, and the error bars are the standard deviations of the measurement. The figure clearly shows that the measured defocuses of the laser pulse agree well with the calculated values for the beam expanders.

Figure 15 shows the spatial and temporal intensity distributions at different positions near the focal plane with and without chromatic aberration. In this calculation, the use of an ideal

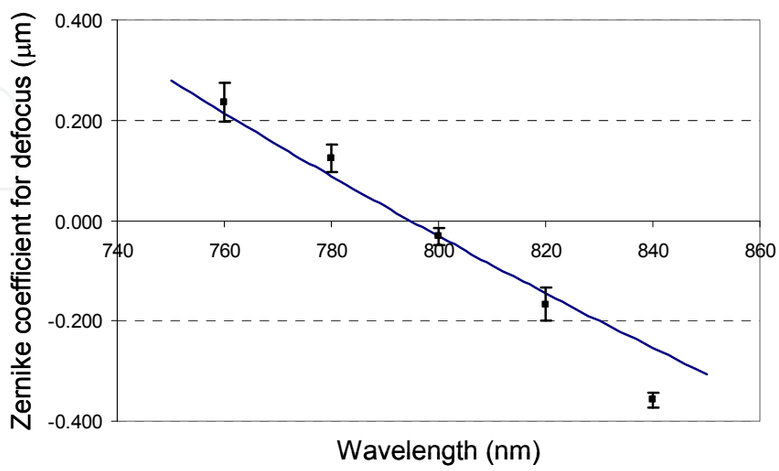

Fig. 14. Change in defocus values when the chromatic aberration of an ultrashort laser beam is not correctly compensated for.

focusing optic having a focal length of 1.5 m is assumed. The change in defocus shown in Fig. 14 was used in the calculations. The monochromatic electric field distributions in the focal plane were calculated in steps of 2 nm over the spectral range, and a focus-shift technique was used to calculate the spatial and temporal intensity distributions at different positions. In Fig. 15, the x-axis of each plot means the time, and the y-axis shows the vertical location at each position. Also, in the figure, by broadening the temporal duration of the focal spot the laser pulse having chromatic aberration showed a very different focusing property than the laser pulse without chromatic aberration. The calculations showed that the peak intensity of the focal spot with chromatic aberration was reduced to about 39% of that of the focal spot without chromatic aberration. The non-symmetric property of the intensity distributions against the focal plane originated from the non-symmetric profile of the laser spectrum. Moreover, with the chromatic aberration, a double-peak structure was observed in several positions near the focal plane. However, the double-peak structure disappeared, recovering to the original pulse duration, when the laser pulse propagated a long distance from the focal plane. Thus, the Fourier transform approach seems to be very useful in calculating the intensity distributions near the focal plane and finally determining the beam propagation properties in both cw and pulsed lasers.

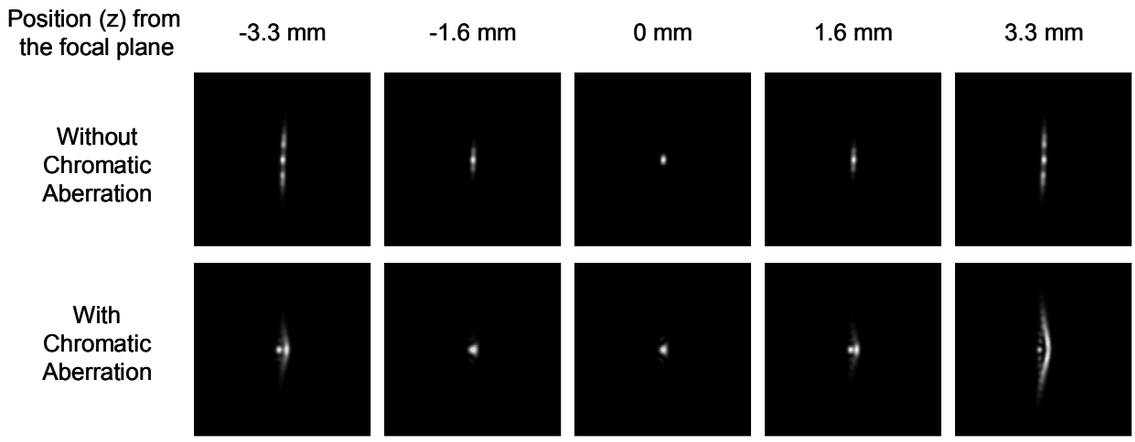

Fig. 15. Spatial and temporal intensity distributions of focal spots at different positions near the focal plane.

4. Beam quality factor

4.1 Definition of beam radius

The propagation of the laser beam can be partially characterized by the beam width and the divergence. In other words, defining the beam quality factor is closely related to the definition of the beam width. For the simple Gaussian laser beam profile, defining the width of the laser beam is trivial. As used in the previous subsections, w_0 and w_1 are used here for the incoming and focused Gaussian beam sizes. However, in some real situations for a complex beam profile with multiple intensity peaks, as shown in Fig. 16, a meaningful and accurate definition of the beam width is not easy. As pointed out by Prof. A. Siegman, there can be many possible definitions of the beam radius for an arbitrary beam profile:

- Width (or half width) at first null

- Transverse knife edge widths
- Width at 1/e or 1/e² in the beam profile
- Radius containing 86% of the entire power
- Second-order moment
- Others

The radius containing 86% of the entire power can be used to calculate the beam propagation of a high-power laser beam in air. The second-order moment is useful to mathematically define the radius of an arbitrary laser beam profile. In the second-order moment, the beam radii for the x- and y-directions are defined by

$$\left\langle w_x^2 \right\rangle = 4\frac{\int_{-\infty}^{\infty}\int_{-\infty}^{\infty} x^2 I(x,y)\,dxdy}{\int_{-\infty}^{\infty}\int_{-\infty}^{\infty} I(x,y)\,dxdy} \text{ and } \left\langle w_y^2 \right\rangle = 4\frac{\int_{-\infty}^{\infty}\int_{-\infty}^{\infty} y^2 I(x,y)\,dxdy}{\int_{-\infty}^{\infty}\int_{-\infty}^{\infty} I(x,y)\,dxdy}. \tag{4.1}$$

In the cylindrical coordinate, the beam radius for a radially symmetrical beam profile is defined by

$$\left\langle w_r^2 \right\rangle = 2\int_0^{\infty}\int_0^{2\pi} r^3 I(r,\varphi)\,drd\varphi \Big/ \int_0^{\infty}\int_0^{2\pi} rI(r,\varphi)\,drd\varphi\,. \tag{4.2}$$

Now, let us calculate the beam radius for a Gaussian laser beam in terms of the second-order moment. For a Gaussian laser beam having a radius w_0, equation (4.2) becomes

$$\left\langle w_r^2 \right\rangle = 2\frac{\int_0^{\infty} r^3 \exp\left(-\frac{2r^2}{w_0^2}\right)dr}{\int_0^{\infty} r\exp\left(-\frac{2r^2}{w_0^2}\right)dr} = 2\frac{\frac{1!}{2}\frac{w_0^4}{4}}{\frac{0!}{2}\frac{w_0^2}{2}} = w_0^2\,. \tag{4.3}$$

And to calculate equation (4.3), we use the definite integral formula

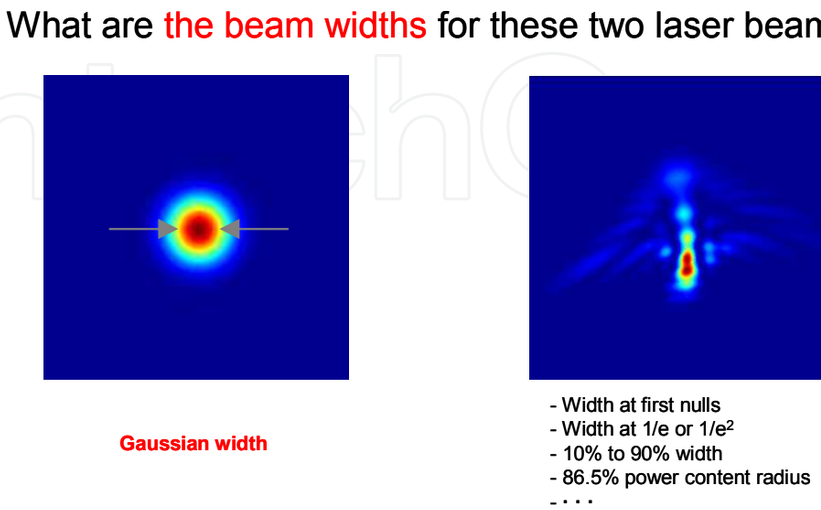

Fig. 16. How to define the beam width for an arbitrary laser beam profile.

$$\int_0^\infty x^{2n+1}\exp\left(-px^2\right)dx = \frac{n!}{2p^{n+1}}\,. \tag{4.4}$$

Thus, for a Gaussian laser beam, we can quickly see the beam radius defined by the second-order moment is again the Gaussian radius w_0. Thus, for a Hermite-Gaussian laser beam of order m and n, equation (4.1) becomes

$$\left\langle w_x^2\right\rangle = (2m+1)w_0^2 \text{, and } \left\langle w_y^2\right\rangle = (2n+1)w_0^2\,, \tag{4.5}$$

where the following integral formulae are used to obtain the expression for equation (4.5):

$$\int_{-\infty}^{\infty} x^2 H_m\left(\sqrt{2}x/w_0\right)\exp\left(-2x^2/w_0^2\right)dx = 2^m\sqrt{\pi}m!\frac{w_0^3}{2^{3/2}}\left(m+\frac{1}{2}\right), \tag{4.6}$$

$$\text{and } \int_{-\infty}^{\infty} H_m\left(\sqrt{2}x/w_0\right)\exp\left(-2x^2/w_0^2\right)dx = 2^m\sqrt{\pi}m!\frac{w_0}{2^{1/2}}\,. \tag{4.7}$$

In the same way, we can calculate the beam radius for a Laguerre-Gaussian laser beam having an arbitrary order. For a Laguerre-Gaussian laser beam, for *p* and *l*, equation (4.2) becomes

$$\left\langle w_{r,pl}^2\right\rangle = (2p+l+1)w_0^2\,. \tag{4.8}$$

For an Airy beam profile ($I(r) = I_0\left[J_1^2\left(kar/f\right)/r^2\right]$), which can be obtained by focusing a flat-top laser beam, equation (4.2) results in

$$\left\langle w_r^2\right\rangle = 2\frac{\int_0^\infty rJ_1^2\left(kar/f\right)dr}{\int_0^\infty \frac{J_1^2\left(kar/f\right)}{r}dr} = \infty\,. \tag{4.9}$$

The numerator in equation (4.9) continuously grows as the radius increases. Thus, as shown in equation (4.9), the radius is not defined for the Airy beam profile in terms of the second-order moment.

4.2 Theoretical determination of the beam quality factor

As mentioned in Section 4.1, the beam quality factor is closely related to the beam propagation. Thus, knowing the intensity distribution near the focal plane is required. Let us begin with equation (3.2) to derive a useful relation for the beam radius with respect to the distance. As shown in equation (3.2), the general expression of the electric field for a laser beam is

$$E_1\left(x_1,y_1,z_1\right) = A\left(z_1\right)\times\exp\left[-ik\frac{x_1^2+y_1^2}{2q\left(z_1\right)}\right], \text{ and } \frac{1}{q\left(z_1\right)} = \frac{1}{R\left(z_1\right)} - i\frac{\lambda}{\pi w_1^2\left(z_1\right)}\,. \tag{3.2}$$

In the plane ($z_1 = z_0$) of the beam waist, $R(z_0) = \infty$ and $\frac{1}{q(z_0)}$ becomes $-i\frac{\lambda}{\pi\langle w_0^2(z_0)\rangle}$.

Then, after a distance z from z_0, the ABCD matrix is given by

$$\begin{bmatrix} A & B \\ C & D \end{bmatrix} = \begin{bmatrix} 1 & z \\ 0 & 1 \end{bmatrix}. \tag{4.10}$$

Next, by using the relation $\frac{1}{q(z)} = \frac{q(z_0)C + D}{q(z_0)A + B}$, we obtain

$$\frac{1}{q(z)} = \frac{1}{R(z)} - i\frac{\lambda}{\pi\langle w^2(z)\rangle} = \frac{1}{z + z_R^2/z} - i\frac{\lambda}{\pi\langle w_0^2\rangle\left[1 + (z/z_R)^2\right]}. \tag{4.11}$$

Again, the definition of the Rayleigh range ($z_R = \pi\langle w_0^2\rangle/\lambda$) is used to derive equation (4.11). From this equation, the beam radius with respect to the distance from the focal plane, z_0, can be expressed by

$$\langle w^2(z)\rangle = \langle w_0^2\rangle\left[1 + \frac{(z - z_0)^2}{z_R^2}\right]. \tag{4.12}$$

Note that equation (4.12) is satisfied for all laser beam modes. From equation (4.12), we know that the change in the size of the beam mode follows a quadratic function with respect to the distance z (after this point, the sign $\langle\ \rangle$ in equation (4.12) will be omitted for convenience). Then, by inserting equations (4.5) and (4.8) into equation (4.12), we can rewrite the beam radii for several laser beams as follows:
For the Hermite-Gaussian beam mode:

$$w_{x,m}^2(z) = W_{0x}^2 + (2m+1)^2\frac{\lambda^2}{\pi^2 W_{0x}^2}(z - z_0)^2 \text{ and } w_{y,n}^2(z) = W_{0y}^2 + (2n+1)^2\frac{\lambda^2}{\pi^2 W_{0y}^2}(z - z_0)^2. \tag{4.13}$$

For the Laguerre-Gaussian beam mode:

$$w_{pl}^2(z) = W_{0,pl}^2 + (2p + l + 1)^2\frac{\lambda^2}{\pi^2 W_{0,pl}^2}(z - z_0)^2. \tag{4.14}$$

Here, W_{0x}^2, W_{0y}^2, and $W_{0,pl}^2$ are defined by $(2m+1)w_0^2$, $(2n+1)w_0^2$, and $(2p+l+1)w_0^2$, respectively. In addition, it should be noted that in real situations the laser beam can have arbitrary beam profile. In this case, it is convenient to generalize the beam radius with respect to the distance as follows:

$$w^2(z) = W^2 + M^4\frac{\lambda^2}{\pi^2 W^2}(z - z_0)^2 \tag{4.15}$$

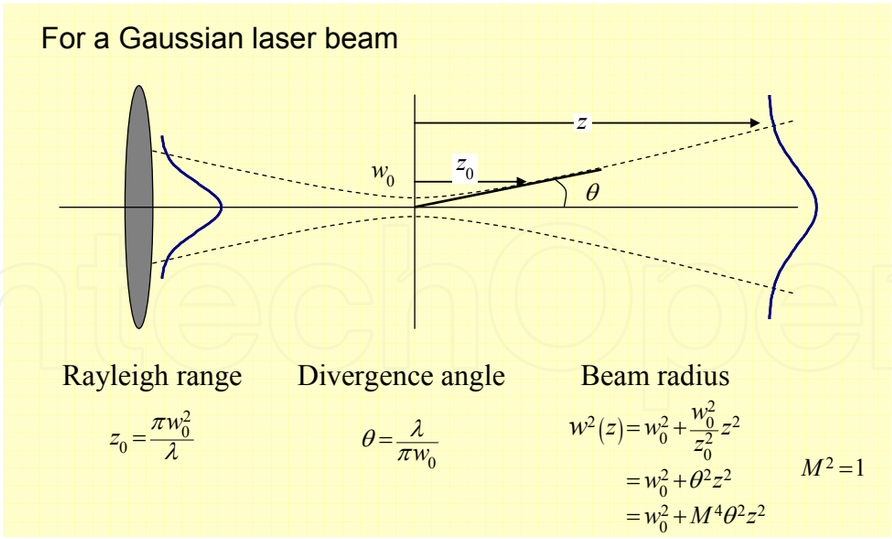

Fig. 17. Beam quality factor, beam radius, divergence angle, and Rayleigh range.

where M^2 is the beam quality factor. From equations (4.13) and (4.14), we can quickly recognize that, for the Hermite-Gaussian and Laguerre-Gaussian beam modes, the beam quality factors are given by $(2m+1)$ and $(2p+l+1)$.

Thus, by using equations (4.1) and (4.2), we can easily derive the property of the radius-divergence product.

$$\left[W^2\theta^2\right] = M^4 \frac{\lambda^2}{\pi^2} \tag{4.16}$$

where θ is the beam divergence defined in Fig. 17. Because the beam quality factor is invariant, it is not affected by the focusing optic once the focusing optic is ideal. In other words, using the invariant property of the beam quality factor, the radius-divergence product remains constant even under different focusing conditions and is given by

$$W_0\theta_0 = W\theta = M^2 \frac{\lambda}{\pi} = \frac{W^2}{Z_0}. \tag{4.17}$$

Finally, from equation (4.17), the beam quality factor for an arbitrary laser beam can be directly calculated by using the second-order moments $W_{x,y}^2$ at the beam waist and the Rayleigh range $Z_{x,y}$:

$$M_x^2 = \frac{\pi W_x^2}{Z_x \lambda} \text{ and } M_y^2 = \frac{\pi W_y^2}{Z_y \lambda}. \tag{4.18}$$

Now, let us calculate the beam quality factor by calculating the beam radii at different positions near the focal plane and the Rayleigh range from the beam radii. In calculating the beam radius, we employ the Fourier transform approach to obtain the intensity distribution, and from the calculated intensity distribution we can calculate the second-order moment as the beam radius. A Gaussian laser beam TEM_{00} is considered first. In this case, the Gaussian

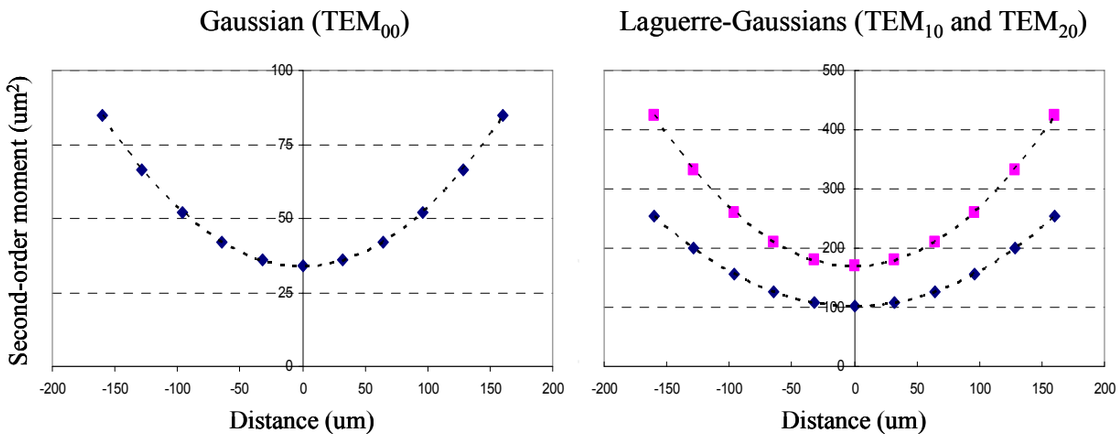

Fig. 18. Calculation of beam radius and the Rayleigh range for Gaussian and higher-order Laguerre-Gaussian (10 and 20) laser beam modes.

width w_1 of the input laser beam was assumed to be 10.337 mm. We also assume that a laser beam having no wavefront aberration is focused by an ideal focusing optic having a focal length of 238 mm, and that the size of the clear aperture of the focusing optic is 70 mm. The large aperture size ensures the extent of the laser beam to be enclosed in the focusing optic. However, the choice of focal length is not important in determining the beam quality factor. The theoretical Gaussian width of the focal spot was about 5.87 μm (calculated from equations (3.10) or (3.39)) at a wavelength of 0.8 μm. In the Fourier transform calculation, the Gaussian width of the focal spot was about 5.82 μm, which is very close to the theoretical width. The calculated second-order moment at the beam waist W^2 and the Rayleigh range Z_0 were about 33.88 μm² and 130.15 μm, respectively. As expected, the second-order moment for the Gaussian beam was given by the square of the Gaussian width. Figure 18 shows the calculated second-order moment for the Gaussian and Laguerre-Gaussian laser beam modes. From the calculated second-order moment and the Rayleigh range, the beam quality factor for a Gaussian beam having no wavefront aberration was calculated as 1.02 using equation (4.18), which is very close to the expected value of 1.00. Subsequent calculations with higher-order Gauss-Laguerre modes showed that the beam quality factors for TEM_{10} and TEM_{20} were 3.04 and 5.08, respectively. The calculated beam quality factors for higher modes were also very close to $(2p+l+1)$, as obtained from the analytical approach. It is thought that the small 1 to 2% error in the beam quality factor comes from calculating the second-order moment.

The beam quality factor for a super-Gaussian beam profile was also investigated because the super-Gaussian beam profile represents the flat-top profile of a real laser beam. Figure 19 shows the normalized intensity profiles and the calculated beam quality factors for Gaussian and super-Gaussian laser beams.

The super-Gaussian orders are 2, 4, 6, 8, 10, 15, 20, 30, and 40 in the calculation. As shown in Fig. 19, the beam quality factor increases with the super-Gaussian order; the beam quality factors for the 30th- and 40th-order super-Gaussian beam profiles are 3.94 and 4.55, respectively. The increase in the beam quality factor with the super-Gaussian order is due to the energy or intensity spread in the focal plane, caused by Airy rings.

With the super-Gaussian intensity profile and a serious wavefront aberration, the intensity distributions at positions -128, -64, 0, 64, and 128 μm from the focal plane are calculated as

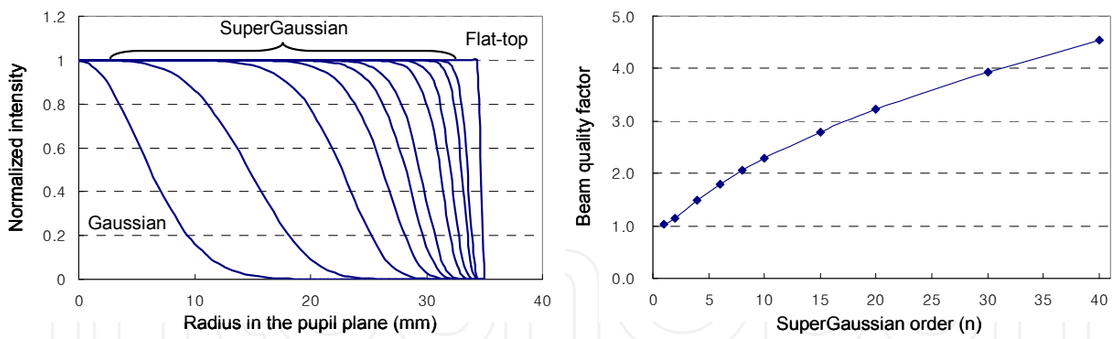

Fig. 19. Intensity profiles of super-Gaussian laser beam modes and the calculated beam quality factors for various super-Gaussian orders.

shown in Fig. 20. The intensity distributions show multiple spikes, and the energy is not well concentrated in a tiny spot because of the wavefront aberration. For these intensity distributions, calculating the second-order moment makes it possible to define the radius of the intensity distribution. In the figure, the blue diamonds and pink squares are the calculated second-order moments $W_x^2(z)$ and $W_y^2(z)$ in the horizontal and vertical directions, respectively. The use of an ideal focusing optic having a focal length of 0.238 m is assumed in this calculation. Again, the dashed line is the second-order polynomial curve fit. The calculated second-order moments for the aberrated laser beam fit the second-order polynomial function well, with the difference between the sagittal and tangential focuses ($z_x - z_y$) being due to astigmatism in the laser pulse. The calculated beam quality factors M_x^2 and M_y^2 for the aberrated laser beam were about 10.1 and 9.9 in the horizontal and the

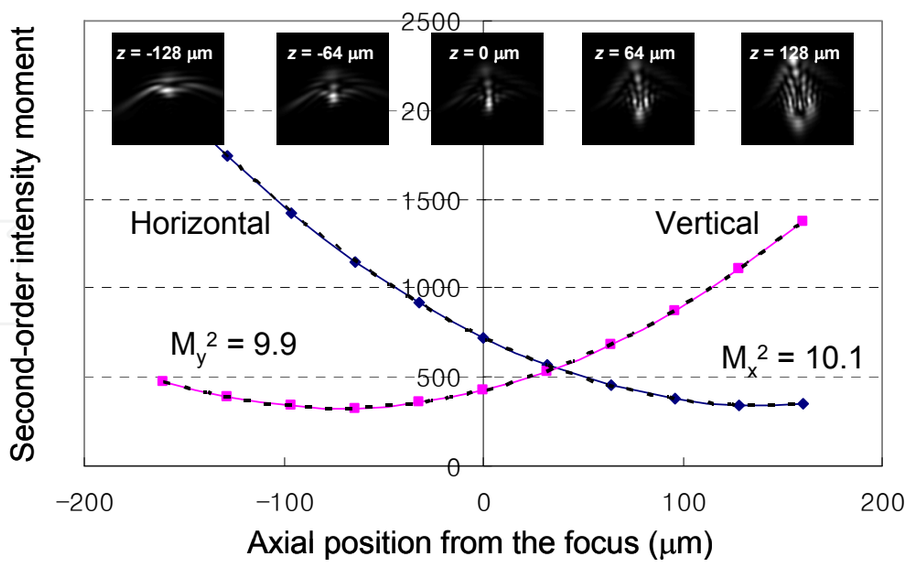

Fig. 20. Calculated intensity distributions and beam radii calculated from the second-order moment. The beam quality factor is then calculated from the beam radii through the second-order polynomial fit.

vertical directions, respectively. The calculated beam quality factors were about 2.6 and 2.5 times higher than those obtained using the same intensity profile having no wavefront aberration. Thus, the beam quality factor can be computationally determined by measuring the intensity of an incoming laser beam and calculating the beam radii at various locations near the focal plane; indeed, calculating the beam radii at various locations is the same procedure as used in the experiment.

4.3 Experimental determination of the beam quality factor

In order to experimentally determine the beam quality factor, measuring the beam radius is first required. For this task, there is a specific instrument, generally called the M-square meter, used to evaluate the beam quality factor. As shown in Fig. 21, the M-square meter basically focuses an incoming laser beam with a relatively long focal length optic. Images at various planes near the focal plane are then recorded by a CCD camera, with beam radii subsequently calculated from the recorded images. Next, from the measured images and the beam radii at various planes, the beam waist and the Rayleigh range can be calculated. Once the beam waist and the Rayleigh range are calculated, the beam quality factor is again given by equation (4.18). Figure 22 shows the image captured from a commercial M-square meter, in which the measured radii at various locations in the M-square meter can be clearly seen. From the measured radii data, the beam quality factor is calculated.

To define the beam diameter, several alternative measurement methods are provided by the International Standardization Office (ISO). In these methods, the beam diameter is defined from the power measurement, instead of the captured image of the laser beam; thus, proper attenuation and accurate calibration of the power meter are necessary. Several measurement methods include: 1) the variable diaphragm method, 2) the moving knife-edge method, and 3) the moving slit method. For the variable diaphragm method, the incoming laser beam can be elliptical but the ratio between the major and the minor axis should be within 1.15:1. The variable diaphragm must be aligned to the beam center to within 10% of the beam diameter. For the knife-edge method, the distance between the energy levels of 10% and 90% should be measured and then multiplied by 1.56. For the moving slit method, a slit having 1/20 width of the laser beam should be used in order to avoid convolution corrections. And, the width between the positions where irradiance has reached 13.5% of the maximum irradiance should be measured.

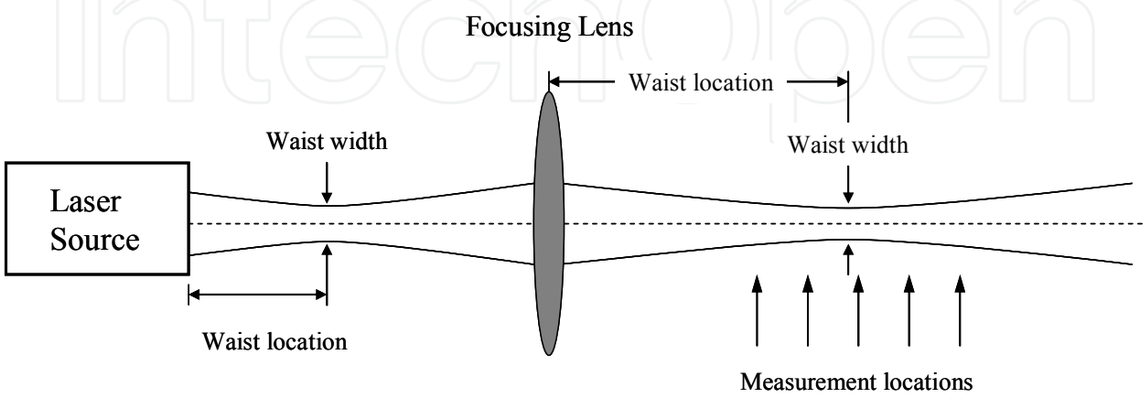

Fig. 21. Optical setup for measuring the beam radii at various locations and determining the beam quality factor.

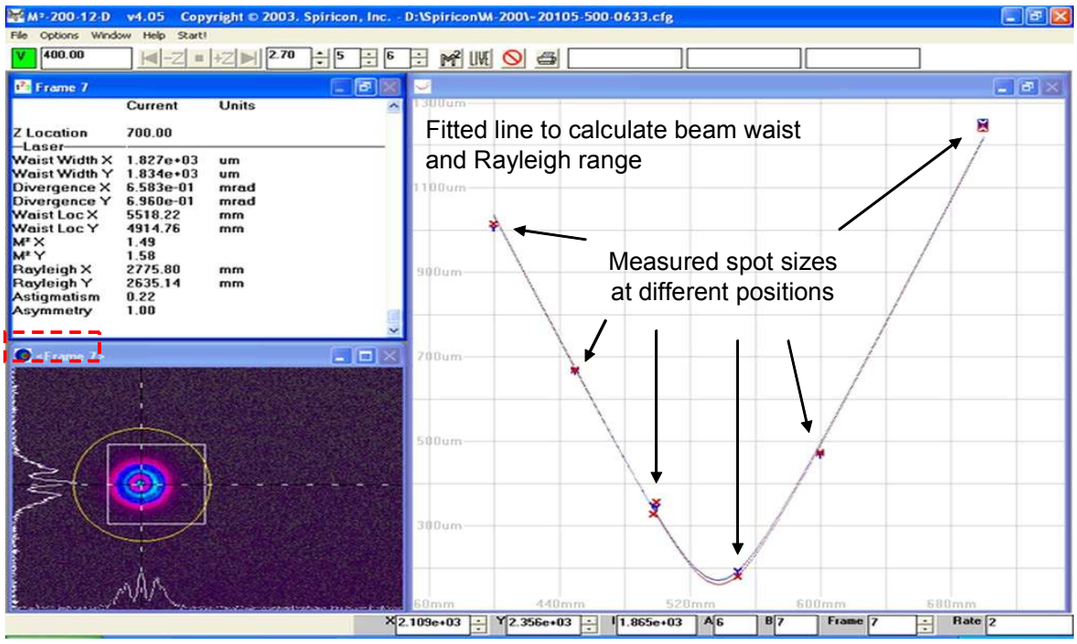

Fig. 22. Measured beam radius and beam quality factor obtained via the M-square meter.

5. Conclusion

The laser pulse has temporal and spatial beam characteristics. The temporal characteristics are related to the pulse duration and the temporal shape of the laser pulse. The spatial characteristics contain the spatial intensity (or electric field) distribution defined by modes and the phase profile of the electric field defined by the wavefront. In order to fully describe the laser pulse in time and space, spatial characteristics such as mode and wavefront should be precisely characterized, in addition to the temporal characteristics. In this Chapter, we describe the intensity distributions as the spatial characteristics of laser beams. In particular, the intensity distribution in the focal plane of a focusing optic or in the vicinity of the focal plane is very important in applications using laser systems because it determines the laser-matter interaction process. We started by deriving the expression for the laser beam intensity and explained the physical background for deriving the mathematical expression of the intensity distribution in the focal plane and in the vicinity of the focal plane. Modification of the intensity distribution with wavefront in the laser beam then followed. Next, the laser pulse was fully characterized in the spatio-temporal domain. The full characterization of the laser pulse quickly introduced a useful concept called the beam quality (or propagation) factor M^2. We also introduced standard methods for experimentally determining the beam quality factor and compared them to an indirect method to determine the beam quality factor based on information pertaining to the intensity and wavefront of the laser pulse. All these topics were discussed under the assumption of the Fraunhofer diffraction region.

6. References

[1] A. E. Siegman, *Laser* (University Science Books, Mill Valley, 1986), Chap. 16.

[2] M. Born and E. Wolf, *Principles of Optics* (Cambridge University Press, Cambridge, 1999), Chap. 8.
[3] P. Milloni and J. H. Eberly, *Lasers* (John Wiley & Sons, New York, 1988), Chap. 14.
[4] O. Svelto and D. C. Hanna, *Principles of Lasers* (Springer, 1998), Chap. 4.
[5] B. E. A. Saleh and M. C. Teich, *Fundamentals of Photonics* (John Wiley & Sons, New York, 1991), Chap. 3.
[6] N. Hodgson and H. Weber, *Laser Resonators and Beam Propagation* (Springer, 2005), Chaps. 2 and 5.
[7] I. S. Gradshteyn and I. M. Ryzhik, *Table of Integrals, Series, and Products* (Academic Press, New York, 2007), Chap. 6.
[8] G. B. Arfken and H. J. Weber, *Mathematical Methods for Physicists* (Academic Press, San Diego, 2001), Chap. 11.
[9] D. Malacara, *Optical Shop Testing* (John Wiley & Sons, New Jersey, 2007), Chaps. 11 and 13.
[10] R. K. Tyson, *Principles of Adaptive Optics* (Academic Press, Boston, 1998), Chap. 5.
[11] A. G. Fox and T. Li, "Resonant Modes in a Maser Interferometer," Bell Sys. Tech. J., 40, 453-488 (1961).
[12] H. Kogelnik and T. Li, "Laser Beams and Resonators," Proc. IEEE, 54, 1312-1329, (1966).
[13] W. H. Carter, "Spot size and divergence for Hermite Gaussian beam of any order," Appl. Opt., 19, 1027-1029 (1980).
[14] J. Durnin, "Exact solutions for nondiffracting beam. I. The scalar theory," J. Opt. Soc. Am. A, 4, 651-654 (1987).
[15] F. Gori, G. Guattari, and C. Padovani, "Bessel-Gauss Beams," Opt. Commun. 64, 491-495 (1987).
[16] D. Wright, P. Greve, J. Fleischer, and L. Austin, "Laser beam width, divergence and beam propagation factor – an international standardization approach," Opt. Quantum Electron. 24, S993-S1000 (1992).
[17] T. M. Jeong, D.-K. Ko, and J. Lee, "Deformation of the Focal Spot of an Ultrashort High-Power Laser Pulse due to Chromatic Aberration by a Beam Expander," Journal of the Korean Physical Society, 52, 1767-1773, (2008).
[18] T. M. Jeong and J. Lee, "Accurate Determination of the Beam Quality Factor of an Aberrated High-Power Laser Pulse," Journal of the Korean Physical Society, 55, 488-494, (2009).

Laser Pulse Phenomena and Applications
Edited by Dr. F. J. Duarte

ISBN 978-953-307-405-4
Hard cover, 474 pages
Publisher InTech
Published online 30, November, 2010
Published in print edition November, 2010

Pulsed lasers are available in the gas, liquid, and the solid state. These lasers are also enormously versatile in their output characteristics yielding emission from very large energy pulses to very high peak-power pulses. Pulsed lasers are equally versatile in their spectral characteristics. This volume includes an impressive array of current research on pulsed laser phenomena and applications. *Laser Pulse Phenomena and Applications* covers a wide range of topics from laser powered orbital launchers, and laser rocket engines, to laser-matter interactions, detector and sensor laser technology, laser ablation, and biological applications.

InTech Europe
University Campus STeP Ri
Slavka Krautzeka 83/A
51000 Rijeka, Croatia
Phone: +385 (51) 770 447
Fax: +385 (51) 686 166
www.intechopen.com

InTech China
Unit 405, Office Block, Hotel Equatorial Shanghai
No.65, Yan An Road (West), Shanghai, 200040, China
中国上海市延安西路65号上海国际贵都大饭店办公楼405单元
Phone: +86-21-62489820
Fax: +86-21-62489821

IntechOpen